Please cite this article in press as: Li et al., The mechanism for thermal-enhanced chaperone-like activity of α-crystallin against UV irradiation-induced aggregation of γD-crystallin, Biophysical Journal (2022), https://doi.org/10.1016/j.bpj.2022.05.032

Biophysical *Journal*
Article

Biophysical Society

The mechanism for thermal-enhanced chaperone-like activity of α-crystallin against UV irradiation-induced aggregation of γD-crystallin

Hao Li,[1,2,3,4] Yingying Yu,[5] Meixia Ruan,[1,4] Fang Jiao,[1,4] Hailong Chen,[1,4] Jiali Gao,[2,3] Yuxiang Weng,[1,4,*] and Yongzhen Bao[5,*]

[1]Laboratory of Soft Matter Physics, Institute of Physics, Chinese Academy of Sciences, Beijing, China; [2]College of Chemical Biology and Biotechnology, Beijing University Shenzhen Graduate School, Shenzhen, China; [3]Institute of Systems and Physical Biology, Shenzhen Bay Laboratory, Shenzhen, China; [4]University of Chinese Academy of Sciences, Beijing, China; and [5]Department of Ophthalmology, Peking University People's Hospital, Eye Diseases and Optometry Institute, Beijing Key Laboratory of Diagnosis and Therapy of Retinal and Choroid Diseases, College of Optometry, Peking University Health Science Center, Beijing, China

ABSTRACT Exposure to solar UV irradiation damages γ-crystallin, leading to cataract formation via aggregation. α-Crystallin, as a small heat shock protein, efficiently suppresses this irreversible aggregation by selectively binding the denatured γ-crystallin monomer. In this study, liquid chromatography tandem mass spectrometry was used to evaluate UV-325 nm irradiation-induced photodamage of human γD-crystallin in the presence of bovine α-crystallin, atomic force microscope (AFM) and dynamic light scattering (DLS) techniques were used to detect the quaternary structure changes of the α-crystallin oligomer, and Fourier transform infrared spectroscopy and temperature-jump nanosecond time-resolved IR absorbance difference spectroscopy were used to probe the secondary structure changes of bovine α-crystallin. We find that the thermal-induced subunit dissociation of the α-crystallin oligomer involves the breaking of hydrogen bonds at the dimeric interface, leading to three different spectral components at varied temperature regions as resolved from temperature-dependent IR spectra. Under UV-325 nm irradiation, unfolded γD-crystallin binds to the dissociated α-crystallin subunit to form an αγ-complex, then follows the reassociation of the αγ-complex to the partially dissociated α-crystallin oligomer. This prevents the aggregation of denatured γD-crystallin. The formation of the γD-bound α-crystallin oligomer is further confirmed by AFM and DLS analysis, which reveals an obvious size expansion in the reassociated αγ-oligomers. In addition, UV-325 nm irradiation causes a peptide bond cleavage of γD-crystallin at Ala158 in the presence of α-crystallin. Our results suggest a very effective protection mechanism for subunits dissociated from α-crystallin oligomers against UV irradiation-induced aggregation of γD-crystallin, at the expense of a loss of a short C-terminal peptide in γD-crystallin.

SIGNIFICANCE α-Crystallin as a small heat shock protein can selectively bind unfolded substrate proteins, hence efficiently suppressing their irreversible aggregation when the structures are destabilized by different denaturing factors. This chaperone-like activity is imperative to maintain the transparency of human lenses. Here, we studied the molecular mechanism of thermal-enhanced chaperone-like activity of bovine α-crystallin against UV irradiation-induced aggregation of denatured human γD-crystallin. We found that the thermal-induced dissociated subunits from α-crystallin oligomer could bind UV irradiation-induced unfolded γD-crystallin forming an αγ-complex, and this newly formed complex could reassociate with the partially dissociated α-crystallin oligomer to prevent aggregation of unfolded γD-crystallin. Thus, a detailed molecular mechanism for thermal-enhanced chaperone-like activity of α-crystallin against UV irradiation-induced aggregation of γD-crystallin is proposed.

INTRODUCTION

The transparency of the eye lens depends on the native tertiary structures and solubility of lens proteins maintained over a lifetime. Crystallins comprise >90% of the total protein in the mature lens (1), among which α-crystallin is the most important water-soluble protein, and its content can

Submitted February 25, 2022, and accepted for publication May 20, 2022.

*Correspondence: yxweng@iphy.ac.cn or drbaoyz@sina.com

Editor: Elizabeth Rhoades.

https://doi.org/10.1016/j.bpj.2022.05.032

Please cite this article in press as: Li et al., The mechanism for thermal-enhanced chaperone-like activity of α-crystallin against UV irradiation-induced aggregation of γD-crystallin, Biophysical Journal (2022), https://doi.org/10.1016/j.bpj.2022.05.032

reach a level as high as approximately 50% of the total structural protein mass in mammalian lenses (2). α-Crystallin, a polydisperse protein complex composed of αA and αB subunits, is a member of the small heat shock protein (sHsp) family (3,4), and it is an ATP-independent chaperone that efficiently binds to damaged or partially unfolded proteins and sequesters them to prevent protein aggregation, which potentially leads to cataract formation (1). α-Crystallin can selectively recognize aggregation-prone nonnative structures that occur early in the denaturation pathway (5,6), and the mechanism of its chaperone function involves the formation of a stable complex between the chaperone and substrate proteins (7). The chaperone-like activity of α-crystallin was discovered over 20 years ago, but even now the molecular mechanism of this chaperone capacity is still far from being understood (8–10).

When isolated from the eye lens, α-crystallin is an oligomeric complex made of αA and αB subunits in a 3:1 ratio (11), which hold together noncovalently to give an averaged molecular weight (MW) of approximately (0.7–1.0) × 10^6 Da (12). The polydisperse oligomer contains 35 to 50 subunits, and these particles are in dynamic equilibrium with small and large sizes (13) by the exchange of subunits (14). Crystal structures of α-crystallin reveal that three consecutive regions generally provide conserved structural organization in sHsps, i.e., an N-terminal region, a core α-crystallin domain and a C-terminal extension (15). The N-terminal region is crucial for substrate binding (15,16), and the flexible C-terminal extension is necessary for stabilization of oligomer structure (15,17), both of which have a positive impact on the regulation of chaperone-like activity (18–22). The conserved α-crystallin domain of the monomer can form the intermolecular antiparallel β-sheets with another monomer (Fig. 1, *A* and *B*), which participates in the assembling of polydisperse oligomers (23). Moreover, oligomerization of α-crystallin monomers leads to interfacial grooves and surrounding pockets, which have been proposed as the hydrophobic substrate binding sites (24). Using protein pin arrays, seven interactive sequences have been identified (25), which overlap with the active residues as reported (26), and one of them is located in strand β6+7, participating in the formation of the dimeric interface. In

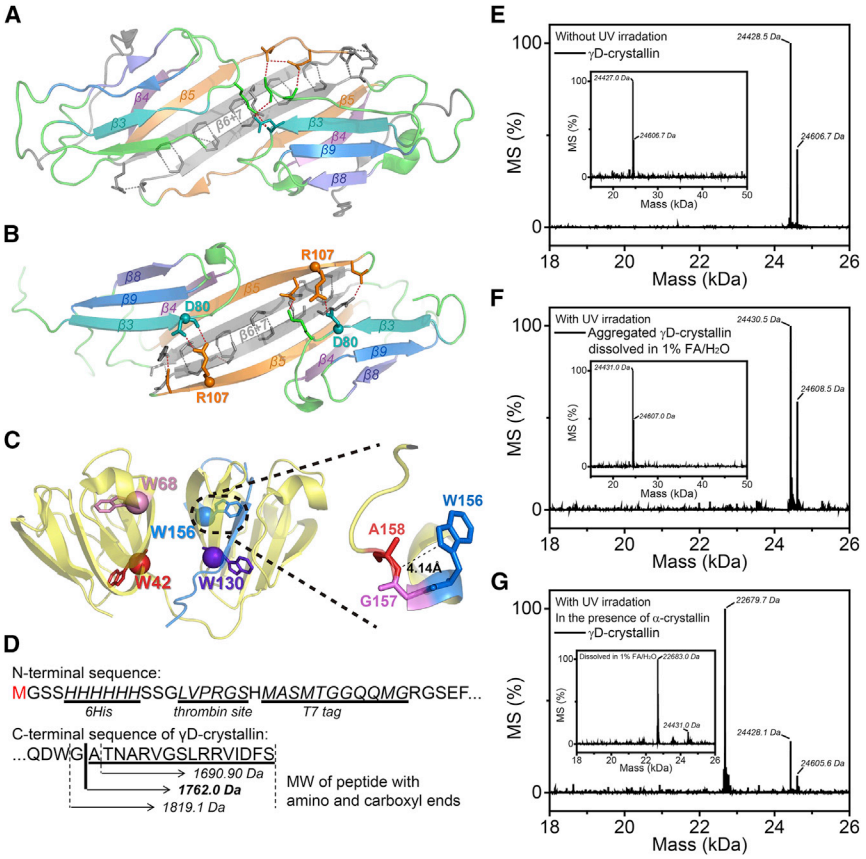

FIGURE 1 Protein structures of dimeric α-crystallin and monomeric γD-crystallin with local structural arrangement around Trp156, and MS spectra of γD-crystallin with or without UV-325 nm irradiation. (*A* and *B*) Dimeric structures of (*A*) human αA-crystallin (PDB: 6T1R) (55) and (B) αB-crystallin (PDB: 2YGD) (57) under neutral condition, with β-strands indicated as β3-9. The intermolecular hydrogen bonds at the dimeric interface are labeled as dashes, including the interaction between the side chains of R(Arg) 107 and D(Asp)80 in human αB-crystallin (*B*). (*C*) The monomeric structure of human γD-crystallin (1HK0) (29) with four conserved Trp(W) residues labeled and its local structures around W(Trp)156-A(Ala)158. The minimum distance between the indole ring of Trp156 and the nitrogen atom next to C_α of Ala158 is 4.14 Å, which makes the radical reaction possible. (*D*) The terminal amino acid sequence of recombinant γD-crystallin. The sites of 6His, thrombin site, and T7 tags at the N-terminus are underlined. The molecular weight (MW) of the short peptide chain containing 15–17 residues is labeled at the C-terminus. M(Met) at the N-terminal end, which tends to be removed by methionyl aminopeptidase during the protein expression, is labeled in red. (*E* and *F*) MW distribution of γD-crystallin without UV irradiation (*E*), and aggregated γD-crystallin upon UV-325 nm exposure (*F*). Photoaggregated γD-crystallin was dissolved in 1% formic acid/H_2O before LC-MS measurement. The MS data were deconvoluted with a 1.0 (*inset*) and 0.5 Da/channel resolution at a mass range of 15–50 (*inset*) and 18–26 kDa, respectively. (*G*) MW distribution of photodamaged γD-crystallin in the presence of α-crystallin. α-Crystallin (50 μM) was mixed with γD-crystallin (41 μM), followed by UV-325 nm irradiation at 40°C, and no protein precipitation can be detected after 30 min UV-325 nm exposure with an average power density of 0.05 W/cm^2. The MS data were deconvoluted from the LC peak of γD-crystallin in Fig. S3 *A*. *Inset*: the photodamaged αγ-oligomer is dissolved in 1% formic acid/H_2O before LC-MS measurement.

Please cite this article in press as: Li et al., The mechanism for thermal-enhanced chaperone-like activity of α-crystallin against UV irradiation-induced aggregation of γD-crystallin, Biophysical Journal (2022), https://doi.org/10.1016/j.bpj.2022.05.032

addition, parts of strand β5 may function as substrate binding sites (27), and this sequence is identified as hydrophobic given the photo-incorporation of a hydrophobic probe (28).

α-Crystallins could assemble into multimeric complexes in the lens and sequester misfolded or damaged γ-crystallins to prevent aggregation, and this passive chaperone capacity decreases with age (3). Specifically, as a monomeric protein in eye lens, γD-crystallin is abundant in the oldest part of the lens, i.e., the nucleus (29). Studies of its folding and unfolding have revealed a partially folded intermediate wherein the N-terminal domain is unstructured, but the C-terminal domain structure is intact (30). The duplicated Greek key structure of γD-crystallin relies on four conserved tryptophan (Trp) residues for thermodynamic stability (Fig. 1 *C*) (31). When ultraviolet light reaches the lens, Trp residues can efficiently funnel UV excitation to thermal energy through a process involving rapid energy transfer and internal conversion, thereby protecting the protein from UV-initiated photochemistry (32–34). However, rare quenching events may lead to UV photodamage, leading to the photochemical cleavage of the polypeptide (35), and molecular oxygen, or reactive oxygen species, may be involved in this photodamage mechanism (36). In realizing the chaperone function, the interaction between α- and γ-crystallins occurs exclusively with the soluble denatured γ-crystallin, and there is at least one potential binding site per subunit of α-crystallin on the protein surface that binds the soluble denatured substrate protein at a stoichiometry of 1:1 for the monomers (37).

α-Crystallin can protect γ-crystallin from UV irradiation-induced aggregation (38–40), and the chaperone function of α-crystallin is thermally activated at temperatures of 30–55°C (41). Owing to the structural irreversibility of partially unfolded bovine α-crystallin after being preheated at higher temperatures (Fig. S1 *A*), the thermal-induced exposure of the hydrophobic surface could be partially retained when cooled to room temperature (RT), which is believed to be responsible for the varied protein protection efficiencies of the preheated α-crystallin (42,43). Vanhoudt et al. have investigated the thermal-induced quaternary structure changes of bovine α-crystallin by inspecting the correlation between the oligomeric size and the corresponding MW against the storage time at 50°C (44). The result indicates that the size and mass of the oligomers are increasing given an increased number of monomers per oligomer, and it also disfavors the molecular aggregation of individual α-crystallin oligomers at a temperature of 50°C. Furthermore, as temperature increases from 4 to 60°C, the thermal effect induces the quaternary and tertiary structure changes, and the partial dissociation of the oligomer to monomers occurs at a lower temperature range, while assembling of the monomer back to the oligomer occurs at higher temperatures (44).

In this work, we employed Fourier-transform infrared spectroscopy (FTIR) and temperature-jump (T-jump) nanosecond time-resolved IR absorbance difference spectroscopy to investigate the thermal-induced secondary structure changes of bovine α-crystallin, evaluated its chaperone-like activity as a function of temperature toward the aggregation of UV irradiation-denatured human γD-crystallin, and examined the protein protection efficiency of the preheated α-crystallin. Temperature-dependent IR absorption spectra in the amide I' band (in D_2O, generally with a red spectral shift of 5–10 cm^{-1} with respect to amide I in H_2O (45)) were resolved into three species-associated spectra by single value decomposition (SVD). These three species are assigned as the most hydrophobic subunits in the inner layer of the oligomer (the major component), the intermediate hydrophobic species as the dissociated subunits in solution, and the most hydrophilic species as the subunits in the outer layer of the oligomer. A typical IR absorption peak at 1604 cm^{-1}, assigned as the absorption of amide carbonyls that participate in the intermolecular hydrogen bonds at the dimeric interface, is used to characterize the thermal-induced dissociation of the subunits from α-crystallin oligomers. This absorption peak reports the breaking of hydrogen bonds and the rearrangement of protein secondary structures as confirmed by FTIR and T-jump time-resolved IR absorbance difference spectra. Thermal dynamic analysis reveals the dissociation of the outer layer subunits from the oligomer at temperatures of 25–55°C, and above 55°C reassociation of the outer layer subunits occurs. Under UV irradiation at a temperature above 35°C, the dissociated subunits bind the unfolded γD-crystallin to form the αγ-complex, and then reassociation of the αγ-complex to the partially dissociated oligomer occurs. This suggests a very effective protein protection efficiency of α-crystallin oligomers against the aggregation of UV irradiation-denatured γD-crystallin. We also evaluate the photodamage of γD-crystallin in the presence of α-crystallin using liquid chromatography tandem mass spectrometry (LC-MS), and the results indicate that a peptide backbone cleavage at Ala158 in γD-crystallin occurs in the αγ-oligomer, leaving a truncated C-terminal peptide of 16 residues in solution. The rationale for preheating α-crystallin above physiological temperature is twofold, i.e., one is to explore the full phase diagram for the thermal stability of bovine α-crystallin, and the other is to provide information to understand the thermal-induced cataract at some special conditions, e.g., cataracts occur frequently among workers who deal with hot materials as a result of exposure to intense infrared radiation, and opacities appear in animal lenses at the critical temperature of 43°C after being heated using microwaves or hot water (46).

MATERIALS AND METHODS

Materials

α-Crystallin (catalog no. C4163) from bovine eye lens was purchased from Sigma-Aldrich (Saint Louis, MO, USA) in the form of a lyophilized powder

Please cite this article in press as: Li et al., The mechanism for thermal-enhanced chaperone-like activity of α-crystallin against UV irradiation-induced aggregation of γD-crystallin, Biophysical Journal (2022), https://doi.org/10.1016/j.bpj.2022.05.032

of high purity as assessed by SDS-PAGE in Fig. S1 *B*. Lyophilized α-crystallins were dissolved into 50 mM phosphate-buffered saline (PBS) buffer (pH 7.4) containing 100 mM NaCl using 3 kDa centrifugal filters (Amicon Ultra-4, Millipore, Saint Louis, MO, USA) followed by adjustment to the indicated concentrations. Before the measurement involving preheat treatment, α-crystallin was first incubated at a given higher temperature for 10 min, then cooled to RT, and kept overnight for equilibration.

Human αB-crystallin and its truncated mutants without terminal extensions ($WT_{truncated}$ and $R107G_{truncated}$) were overexpressed from the plasmid (pET-28a) using *Nde*I and *Bam*HI as restriction sites. After nickel affinity purification with 5 mL HisTrap excel column, thrombin (I8040, Solarbio, Beijing, China) was added for cleavage of His-tag. Further FPLC purification was performed on the size-exclusion column (Superdex 200 Increase 10/300 GL, Cytiva, Marlborough, MA, USA) to remove the His-tag.

Human γD-crystallin containing 6×His-tag, thrombin site, and T7 tag at the N-terminus was prepared as described previously (47). In brief, the recombinant plasmids (pET-28a) using *Eco*RI and *Xho*I as restriction sites were transformed into *E. coli* BL21(DE3) competent cells, and the proteins were purified by nickel affinity chromatography on an AKTA purification system. After column elution with 0.5 M imidazole, the collected samples were desalted into 50 mM PBS buffer (pH 7.4) containing 100 mM NaCl and adjusted to the indicated protein concentrations. The amino acid sequences of human αB- and γD-crystallins with N-terminal tags are listed in Fig. S2.

For preparation of photodamaged αγ-oligomer, 50 μM α-crystallin was mixed with 41 μM γD-crystallin, followed by UV-325 nm irradiation at 40°C with an average power density of 0.05 W/cm^2 for 30 min. The electrophoretogram is displayed in Fig. S1 *B*.

Chaperone activity assays

(1) Temperature-dependent chaperone-like activity of α-crystallin was determined by measuring the turbidity of a solution containing bovine α- and human γD-crystallins under UV irradiation. The laser used for irradiation was generated by a He-Cd laser emitting at 325 nm (IK3301R-G, Kimmon Koha, Tokyo, Japan) with an average power density of 1 W/cm^2 at the sample position, with the irradiation size fourfold smaller than the one used in the preparation of photodamaged αγ-oligomer. A Si-based detector (DET100A/M, Thorlabs, Nuneaton, UK) connected to a digital oscilloscope was used to record the intensity of scattered light every 6 s. The aqueous solution was loaded in a CaF_2 sample cell with 300- and 50-μm thick Teflon spacers at different protein concentrations of 20.5 and 164 μM for γD-crystallin, respectively, and the ambient temperature was controlled by a water circulator with an accuracy of 0.2°C.

(2) Tris(2-carboxyethyl) phosphine (TCEP)-induced aggregation of insulin was measured as a function of time with or without the preheated α-crystallin by monitoring the apparent absorption at 400 nm at RT. TCEP (catalog no. 75259) and insulin (catalog no. I5500) were purchased from Sigma-Aldrich. Bovine α-crystallin in 50 mM PBS buffer (pH 7.4, containing 100 mM NaCl) was first equilibrated at the required temperature for 10 min, then cooled to RT, and mixed with insulin. The reduction of disulfide bonds was initiated by adding 3 μL of 80 mM TCEP to 180 μL of insulin at a protein concentration of 34.8 μM, and the aggregation reflected by scattered light was monitored in a microplate reader (Multskan GO, Thermo, Waltham, MA, USA).

The chaperone-like activity of α-crystallin was evaluated as a percentage of protein protection against aggregation using the formula of protein protection efficiency (%) = $((A_0 - A)/A_0) \times 100$, where A_0 and A represent the intensity of light scattering after a duration at a given temperature with or without α-crystallin, respectively (41). The measurements were repeated at least thrice to verify the reproducibility, and standard error bars were derived from three individual measurements.

Fluorescence measurements for protein surface hydrophobicity

α-Crystallin was first incubated at the indicated temperature for 10 min and cooled to RT. Then concentrated protein-bound 4,4′-dianilino-1,1′-binaphthyl-5,5′-disulfonic acid dipotassium salt (bis-ANS) was added (Sigma-Aldrich, catalog no. D4162). The preheated α-crystallin (5 μM) was incubated with 25 μM bis-ANS with gentle stirring in the dark for at least 1 h at 25°C, and the fluorescence spectra of bis-ANS were measured on F-4500 spectrometer (Hitachi, Tokyo, Japan) with an excitation wavelength of 390 nm (27,32). All measurements were performed in 50 mM PBS buffer (pH 7.4, containing 100 mM NaCl) at RT with gentle stirring.

Dynamic light scattering and atomic force microscope measurements of protein quaternary structures

For dynamic light scattering (DLS) measurement, α-crystallin and photodamaged αγ-oligomer (10 μM for α subunits) were first incubated in 50 mM PBS buffer (pH 7.4, containing 100 mM NaCl) at 40°C for 30 min to realize the thermal equilibration. Hydrodynamic size distribution was measured using DynaPro Nanostar (Wyatt Technology, Santa Barbara, CA, USA) with at least 45 repetition for calculations. Atomic force microscope (AFM) was applied in the characterization of oligomeric quaternary structure. Incubated samples (5 μL), at protein concentrations of 0.5 μM for α subunits, were directly added on small freshly cleaved mica disk (2 mm in diameter) with 7 min equilibrium, followed by sufficiently rinsing with a buffer of 20 mM Hepes-NaOH (pH 7.4) and 150 mM NaCl. All images were acquired in the above rinsing buffer using silicon probes (HYDRA6V-100NG, k = 0.292 N/m, AppNanon ScanAsyst mode with a Multimode 8 AFM (Bruker Optics, Madison, WI, USA) and the quaternary structure was characterized by equivalent diameter of the oligomers.

LC-MS measurement for UV irradiation-induced photodamaged products

LC-MS data were collected using ultra performance liquid chromatography coupled time-of-flight mass spectrometry (SYNAPT XS, Waters, Milford, CT, USA) for high-resolution MW of peptides. α-Crystallin and photodamaged αγ-oligomer were diluted to 10 μM for α subunits with H_2O, and photoaggregated γD-crystallin was dissolved in 1% formic acid/H_2O at the same protein concentration. The sample (1 μL) was loaded onto the ultra performance liquid chromatograph and separated by a MAbPacTM RPLC column (3.0 × 100 mm, 4 μm, Thermo Fisher Scientific, Waltham, MA, USA) at 40°C. Solvent A was 0.1% formic acid/H_2O and solvent B was 100% acetonitrile, and a step gradient from 10 to 95% of solvent B over 10 min was applied at a flow rate of 0.2 mL/min. The scan mode was set as sensitive with MS scan range at 100–2000 m/z. The data were analyzed using MassLynx V4.2 software and deconvoluted with a 1.0- and 0.5-Da/channel resolution at a mass range of 15–50 and 18–26 kDa, respectively.

FTIR measurement of protein secondary structures

For infrared spectroscopic experiments, the lyophilized α-crystallins were dissolved in 50 mM PBS buffer (pH 7.4), which was prepared in D_2O, with a final NaCl concentration of 100 mM. Temperature-dependent FTIR absorption spectra were acquired on a spectrometer (VERTEX 70V, Bruker Optics, Madison, WI, USA) at a protein concentration ranging from 80 to 800 μM, and the thermal-induced secondary structure changes of bovine α-crystallin were independently assessed at different protein concentrations (Fig. S1 *C*). A two-compartment CaF_2 sample cell with a

Please cite this article in press as: Li et al., The mechanism for thermal-enhanced chaperone-like activity of α-crystallin against UV irradiation-induced aggregation of γD-crystallin, Biophysical Journal (2022), https://doi.org/10.1016/j.bpj.2022.05.032

50-μm-thick Teflon spacer was used for simultaneously loading the sample and reference. The measurement was performed in a home-built vacuum chamber equipped on FTIR spectrometer, and the temperature was controlled by a water circulator (48–50). Each spectrum was recorded in the 1000–4000-cm^{-1} region at a resolution of 0.2 cm^{-1} and 60 scans were signal averaged. Second derivative analysis based on the absorption spectra provided a better spectral resolution with an enhancement factor of 1.88 for a Gaussian type of lineshape (51), and the negative peaks in the second derivative spectrum (with its magnitude corresponding to the absorption intensity) were used for the assignment of absorption peaks in the FTIR spectrum.

T-jump nanosecond time-resolved IR absorbance difference spectra for thermal-induced protein unfolding

The details of T-jump time-resolved IR absorbance difference spectrometer have been described previously (50,52). In the current apparatus, a 1.9-μm pulsed laser generated from a home-built Q-switched Cr, Tm, Ho:YAG laser, was used as a laser heating source, which induced a rapid increase in temperature from 25 to 35°C for the solvent, as calibrated by the temperature-dependent FTIR spectra of D_2O. IR absorbance changes were probed using a CO mid-IR laser at a spectral spacing of approximately 4 cm^{-1} in conjunction with an MCT detector (Kolmar, Newburyport, MA) and a digital oscilloscope (Tektronix, TDS520D, Santa Clara, CA). The detection limit of the T-jump transient IR absorbance difference spectra is approximately 2×10^{-4} ΔOD, and the temporal resolution of this system is approximately 80 ns. The protein concentration of bovine α-crystallin was maintained at 400 μM for the measurement.

RESULTS

LC-MS analysis of UV irradiation-induced photodamage of γD-crystallin

γD-Crystallin, one of the three major γ-crystallins required for lens transparency, was used as the substrate as it can be photoaggregated upon UV exposure. Direct UV exposure of γD-crystallin causes Trp and Cys oxidation in the presence of oxygen (36). When Trp residues absorb ultraviolet light, it can result in the opening and oxidation of the indole ring (31), and the net effect would be the exposure of hydrophobic residues and the cleavage of the peptide backbone (35). When Trp (W) residues in γD-crystallin were replaced by Glu (E), the αB-crystallin chaperone suppressed the aggregation of W130E, but not W42E (31), indicating that the intermolecular binding sites for γD-crystallin would locate at the N-terminal domain that comprises W130. In this study, we investigated UV-325 nm irradiation-induced photodamage of γD-crystallin based on LC-MS analysis, and explored the relationship between Trp residues and the cleavage of the polypeptide backbone of γD-crystallin in the presence of α-crystallin.

As shown in Fig. S3 *A*, two peaks appear in the LC of bovine α-crystallin, which represent αB and αA subunits, respectively, and the corresponding MW distribution is displayed in Fig. S3, *B* and *C*. The αB subunit exhibits two peaks in the MS spectrum, i.e., at 20,080.2 and 20,160.0 Da, and the αA subunit exhibits peaks at 19,833.5 and 19,914.1 Da. For each α subunit, the smaller MW corresponds to the intact bovine αB and αA subunits, respectively, and the larger weight is derived from one phosphorylation with an increased mass of ∼80 Da, well consistent with the reported results by Han et al. (53), i.e., the MW for intact bovine αA- and αB-crystallin is 19,832 and 20,080 Da, respectively, by the matrix-assisted laser desorption ionization mass spectrum. The MW of γD-crystallin was identified in Fig. 1 *E*, and this subunit containing 6×His-tag, thrombin site, and T7 tag at the N-terminus exhibits two peaks at 24,428.5 Da (major) and 24,606.7 Da (minor). The calculated MW of human γD-crystallin containing N-terminal tags with a loss of Met is 24,427.1 Da, corresponding to the loss of Met at the N-terminal end as removed by methionyl aminopeptidase during protein expression (Figs. 1 *D* and S2). The minor peak at 24,606.7 Da matches the tagged γD-crystallin with three oxidation sites (calculated MW: 24,606.3 Da). We also investigated UV-325 nm irradiation-induced photodamage of α- and γD-crystallins using LC-MS, respectively. As shown in Figs. S3, *D*, *E*, and 1 *F*, the MW distribution of both individual crystallins has almost no change upon UV exposure, which indicates a high resistance of the peptide integrity of both α- and aggregated γD-crystallins on the UV-325 nm irradiation.

Further exploration of the photodamage of γD-crystallin is detected in the presence of α-crystallin. The mixture of α- and γD-crystallins was irradiated with UV-325 nm light at 40°C, and the photodamaged products were identified based on the LC-MS spectra (Figs. S3 *A* and 1 *G*). The difference in the MW distribution of the crystallin mixture under UV irradiation is mainly reflected in the decreased peak at 24,428.1 Da (together with 24,605.6 Da) and an intense new peak at 22,679.7 Da (Fig. 1 *G*), both of which are deconvoluted from the LC peak of γD-crystallin (Fig. S3 *A*). According to the amino acid sequence of recombinant γD-crystallin (Fig. S2), the newly formed peptide with the MW of 22,679.7 Da is derived from the photolytic cleavage of the backbone at Ala158 (C_α-N), and this cleavage is related to the formation of an indolyl radical (36) at Trp156 (Fig. 1 *C*). The mass difference between the recombinant γD-crystallin (24,428.1 Da) and the newly formed peptide (22,679.7 Da) is 1748.4 Da (Fig. 1 *G*), and the calculated MW of the C-terminal peptide "ATNARVGSLRRVIDFS" without the amino end is 1748.0 Da (Fig. 1 *D*).

Thermal-enhanced chaperone-like activity of bovine α-crystallin

To reproduce the thermal-enhanced chaperone-like activity of bovine α-crystallin, we investigated the photo-induced aggregation of γD-crystallin with or without α-crystallin at temperatures of 25–65°C using a He-Cd laser emitting at 325 nm as the UV light and evaluated the protein protection efficiency as a function of temperature. As shown in Fig. S4, *A* and *B*, α- and γD-crystallins at different temperatures

Please cite this article in press as: Li et al., The mechanism for thermal-enhanced chaperone-like activity of α-crystallin against UV irradiation-induced aggregation of γD-crystallin, Biophysical Journal (2022), https://doi.org/10.1016/j.bpj.2022.05.032

were irradiated separately as a control, which shows that UV-325 nm irradiation-induced aggregation of bovine α-crystallin is negligible at temperatures of 25–65°C, while γD-crystallin is gradually aggregated, and the extent of its aggregation is further enhanced as temperature increases (Fig. S4, *A* and *B*). In contrast, the mixed protein solution in the presence of α-crystallin exhibits a minimum turbidity at a temperature of approximately 55°C (Fig. S4, *C* and *D*), which reflects a maximum protection efficiency as shown in Fig. 2 *A*. Moreover, the turbidity of the solution at different temperatures is affected by the change of a molar ratio between γD- and α-crystallins (Fig. S4 *D*), and such a tendency of the temperature-dependent protein protection efficiency is still valid at a higher protein concentration of 164 μM (Fig. 2 *A*).

It has been suggested that the chaperone-like activity of α-crystallin is correlated with the hydrophobic binding of the substrates (42). However, whether this hydrophobic interacting surface is already exposed or freshly exposed as temperature increases has not been determined yet. To address this issue, we examined the protein protection efficiency of preheated α-crystallins against UV-325 nm irradiation-induced aggregation γD-crystallin and TCEP-induced aggregation of insulin at RT (Fig. 2 *B*). Given the thermal-induced irreversibility of partially unfolded protein structures at a higher temperature, parts of the newly formed solvent-exposed hydrophobic structures would remain when cooled to RT (Fig. S1 *A*). In the measurement of the protein protection efficiency, preheated α-crystallins, which were first equilibrated at the given temperatures for 10 min then cooled to RT, were mixed with the substrates at the indicated protein concentrations, followed by at least 30 min incubation in the dark. The TCEP-induced aggregation of insulin was generated from the reduction of disulfide bonds, and the turbidity derived from the absorbance at 400 nm was monitored as a function of time. As shown in Fig. S5, *A* and *C*, TCEP cannot precipitate the preheated bovine α-crystallin at RT, thus, the turbidity that can be measured is completely derived from the aggregation of the insulin B chain (42,54).

We further characterize the unrecovered thermal-induced exposed hydrophobic surface in the preheated α-crystallin using a hydrophobic bound fluorescence probe molecule bis-ANS, and the fluorescence emission spectra are shown in Fig. 2 *C*, which reveal that the fluorescence intensity increases with the temperature for preheat (*inset* of Fig. 2 *C*), and the maximum intensity at 492 nm reflects the proportion of the unrecovered thermal-induced exposed hydrophobic surface. Fig. 2 *D* plots the preheat temperature-dependent protein protection efficiency of α-crystallin against UV-325 nm irradiation-induced aggregation of γD-crystallin and TCEP-induced aggregation versus the corresponding fluorescence intensity of bis-ANS, and both of them show a good linear correlation. Therefore, our results suggest that the thermal-induced substrate binding occurs at the freshly exposed hydrophobic surface.

IR spectroscopic characterization of thermal-induced secondary structure changes

The temperature-dependent IR absorption spectra and the corresponding second derivative spectra of bovine

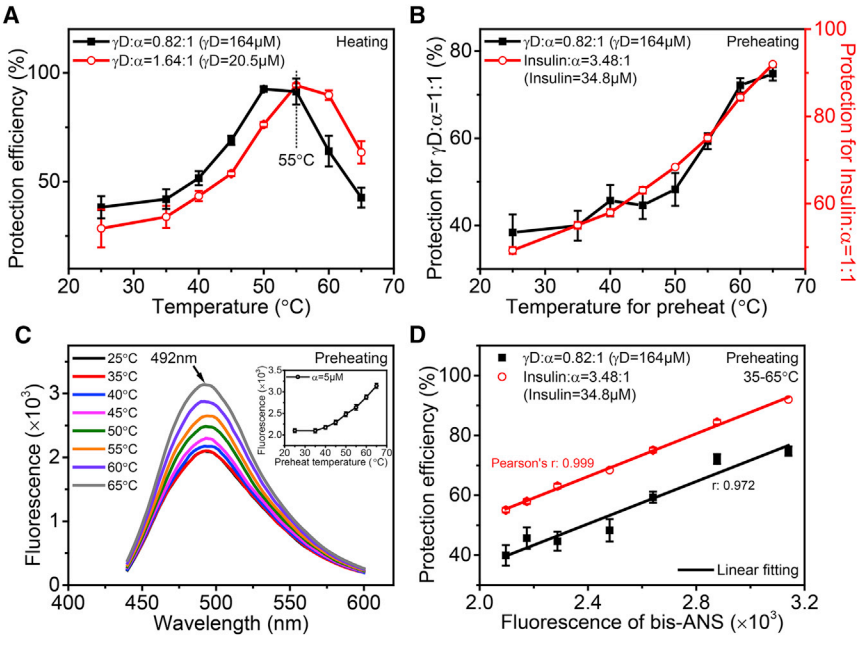

FIGURE 2 Temperature-dependent protein protection efficiency of bovine α-crystallin and its linear correlation with the surface hydrophobicity after preheat treatment. (*A*) Chaperone-like activity of bovine α-crystallin against heating temperature. The measurements were performed using 164 and 20.5 μM γD-crystallin as the substrate protein, and the chaperone-like activity was evaluated using the formula of protein protection efficiency (%) = $((A_0 - A)/A_0) \times 100$, where A and A_0 represent the turbidity of the solution after a duration of exposure to UV light at the given temperatures with or without bovine α-crystallins. (*B*) Protein protection efficiency of preheated α-crystallins against aggregation of UV irradiation-denatured γD-crystallin and TCEP-induced aggregation of insulin at RT. α-Crystallin were first incubated at a given higher temperature for 10 min, then cooled to RT, and kept overnight for equilibration. Preheated α-crystallins were mixed with the substrates at the indicated protein concentrations, and incubated at least 30 min in the dark, followed by the measurements at RT. (*C*) Preheat temperature-dependent fluorescence spectra of protein-bound bis-ANS. The preheated α-crystallin was incubated with 25 μM bis-ANS at a protein concentration of 5 μM followed by excitation at 390 nm. The maximum fluorescence intensity at 492 nm against the temperature for preheat is present in the graphic inset. (*D*) Linear correlations between the fluorescence intensity of protein-bound bis-ANS at 492 nm and the protein protection efficiency against aggregation of denatured γD-crystallin and insulin.

Please cite this article in press as: Li et al., The mechanism for thermal-enhanced chaperone-like activity of α-crystallin against UV irradiation-induced aggregation of γD-crystallin, Biophysical Journal (2022), https://doi.org/10.1016/j.bpj.2022.05.032

α-crystallin in D_2O are shown in Figs. S6 and 3 *A*, and the absorption peaks in the amide I′ band can be better resolved in their second derivative spectra as negative peaks. The absorption at 1628 (intense) and 1685 cm^{-1} (weak) are typical finger prints for the antiparallel β-sheets existing in α-crystallin (55–57) (Fig. 3 *A*), which are derived from the strong coupling between carbonyl groups in the adjacent peptide chains (45,58–60). In the previous reports, the peak centered at about 1604 cm^{-1} has been assigned to the intermolecular hydrogen bonds between amino acids, e.g., the absorption of the asymmetric stretching motion of COO^-, which forms an intermolecular hydrogen bond with the NH_3^+ group in amino acid (His and Gly) D_2O solutions (61), C=O stretching vibration in N-H···O=C hydrogen-bonded networks induced by high pressure (62), or the side-chain vibration of Arg and Tyr in D_2O (63,64). Gruszecki et al. investigated the intermolecular interactions of light-harvesting pigment-protein complex LHCII in the monomolecular films formed at the argon-water interface by FTIR (65). They showed that the organization of LHCII trimers within a monolayer was associated with formation of intermolecular hydrogen bonds between neighboring polypeptides with a typical IR absorption band at 1609 cm^{-1}. This spectral feature has also been observed in aggregated LHCII trimers at 1610 cm^{-1} by our group (50). Lin et al. investigated the secondary structure of bovine α-crystallin in different buffer solutions (pH 2.2, 4.0, 6.0, 7.2, and 8.0) by attenuated total reflection/FTIR spectrometry in H_2O (66). They found that a 1611 cm^{-1} peak exists in solutions of all the different pH values except for that at pH 2.2. Since, at pH 2.2, the oligomer of α-crystallin dissociated completely, this gives a straightforward evidence that the 1611 cm^{-1} peak is from the binding interfaces. In addition, the assignment of the 1604 cm^{-1} band to the absorption of intermolecular hydrogen bonds between antiparallel β-sheets is further verified by our IR spectra of human αB-crystallin and its mutants. As shown in Fig. 3 *B*, the second derivative IR spectra of αB-crystallin with and without terminal extensions were acquired at RT. The similar absorption at 1604 cm^{-1} between αB-crystallin and its truncated mutant indicate that the intermolecular hydrogen bonds are mainly located in the core α-crystallin domain but not in the terminal structures. We also compared the second derivative IR spectra of truncated αB-crystallin domain with its mutant R107G. A pair of IR absorption bands around 1625 and 1680 cm^{-1} assigned as the antiparallel β-sheet structures for truncated αB-crystallin are apparently red shifted with respect to that of intact αB-crystallin, indicating that the truncated structure is more hydrophilic. Based on the crystal structure of human αB-crystallin (Fig. 1 *B*), the side chain of R107 interacts with D80 from the adjacent subunit at the dimeric interface via intermolecular hydrogen bond, and the mutation from Arg to Gly would break this interaction, leading to the decreased IR absorption at 1604 cm^{-1}, as observed in Fig. 3 *B*. Therefore, the 1604 cm^{-1} peak in D_2O is thus assigned as the absorption from hydrogen bonds at the dimeric interface within the oligomers. The intensity of the negative peak at 1604 cm^{-1} corrected by that of the background at 1595 cm^{-1} (I_{1604}-I_{1595}) in the second derivative spectra against the temperature is given in Fig. 3 *C*, and the monotonous decrease of the second derivative intensity suggests a continuous breaking of the intermolecular hydrogen bonds at the dimeric interface (the magnitude of the negative peak in the second derivative spectrum corresponds to the absorption intensity). This second derivative intensity (negative value) at 1604 cm^{-1} (I_{1604}-I_{1595}) for the preheated α-crystallin is also plotted against the temperature for preheat, as shown in Fig. 3 *C*, which shows that the hydrogen bonds at the dimeric interface are almost completely recovered after preheat treatment at a temperature below 49°C, and the difference absorption, which is interpreted as the irreversible dissociated subunits in solution, increases significantly when the temperature for preheat exceeds 49°C. As the relative amplitude (I_{1604}-I_{1595}) corresponds to the amount of unbroken hydrogen bonds ($N_{H\text{-}unbroken}$), the equilibrium constant for the breaking of hydrogen bonds at different heating temperatures ($K_{H\text{-}bond}(T)$) can be expressed in a ratio between the amount of broken ($N_{H\text{-}broken}$) and unbroken ($N_{H\text{-}unbroken}$) hydrogen bonds as $K_{H-bond}(T) = \frac{N_{H-broken}(T)}{N_{H-unbroken}(T)} = \frac{N_{H-unbroken}(25^\circ C) - N_{H-unbroken}(T)}{N_{H-unbroken}(T)}$. With the van 't Hoff equation, i.e., (67,68), thus the entropy ($\Delta H_{H\text{-}bond}$) and enthalpy ($\Delta S_{H\text{-}bond}$) changes for breaking the intermolecular hydrogen bonds at the dimeric interface can be derived. Fig. 3 *D* plots ln $K_{H\text{-}bond}(T)$ versus $1/T$ from 37 to 67°C, which can be well fitted by a straight line. This result suggests a continuous disruption of hydrogen bonds at the dimeric interface in such a large wide temperature span, and the corresponding $\Delta H_{H\text{-}bond}$ is 22.6 ± 0.9 kcal mol^{-1} and $\Delta S_{H\text{-}bond}$ is 64.5 ± 2.8 cal mol^{-1} K^{-1}.

SVD analysis to resolve thermal-induced dissociation and reassembly of subunits

To elucidate the thermal-induced effect on the structural changes of bovine α-crystallin, SVD analysis, which has been proven to be a powerful mathematical method in spectral resolution for resolving individual species-associated components from mixed spectral contributions (48,49,69), is used to resolve the species-associated spectra and evaluate the populations of different structural components, according to the procedure used in resolving the species-associated IR absorption spectra of β-crystallin (48). Bovine α-crystallin with two subunits (αA and αB) is considered as a heteroligomer. SVD analysis is performed on the matrix composed of IR spectra at different temperatures to obtain the singular values of the major components. As shown in Fig. S7 *A*, the first six coefficients of the major components are displayed in a descending order, where the first three are significantly larger than others, which justifies that

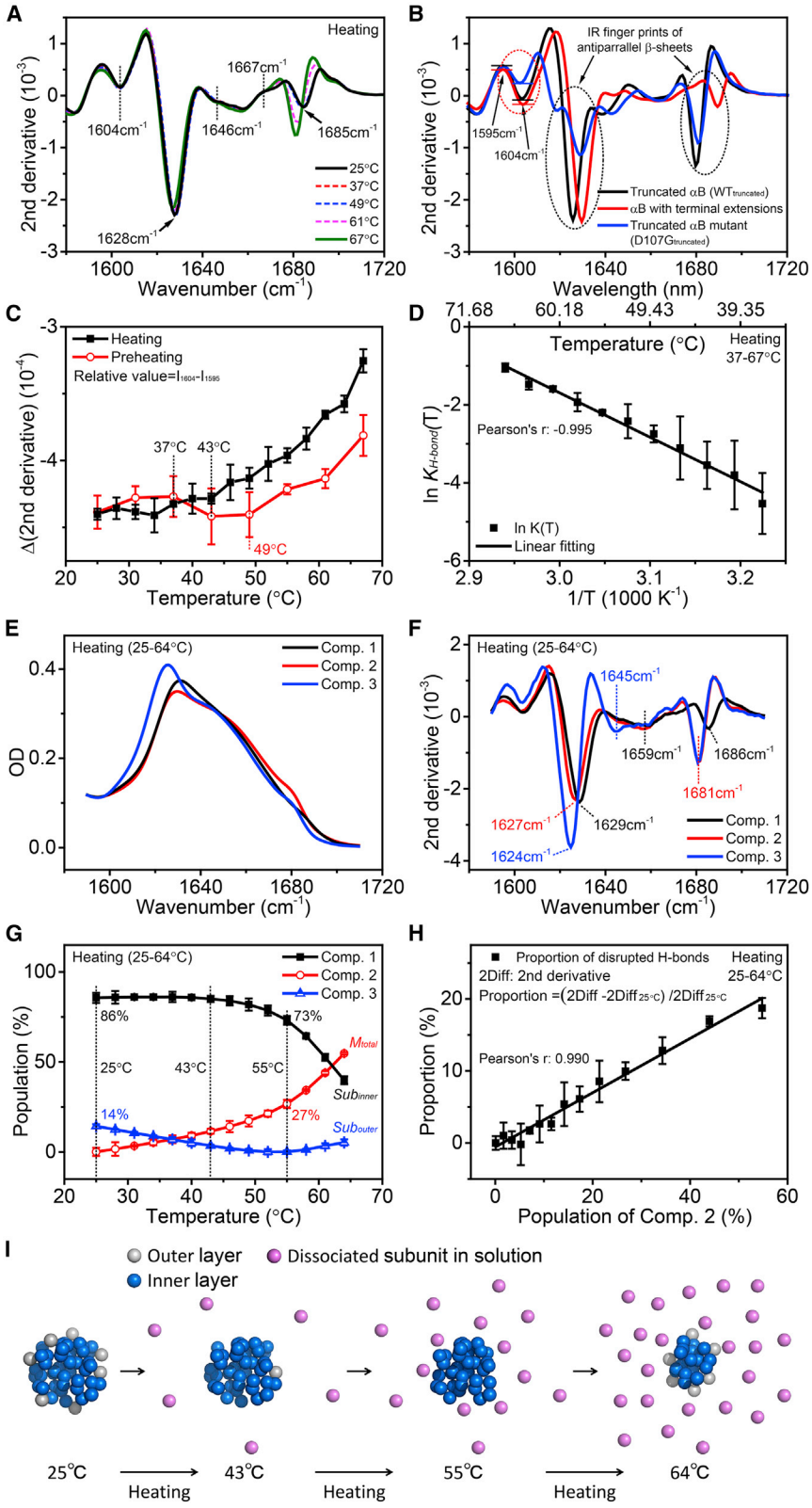

FIGURE 3 IR absorption spectra of α-crystallin and the linear correlation between the temperature-dependent SVD-resolved population of intermediate component (component 2) and the proportion of disrupted intermolecular hydrogen bonds at the dimeric interface. (*A*) Second derivative FTIR spectra of bovine α-crystallin at the indicated temperatures. The magnitude of the negative peak in the second derivative spectrum corresponds to the absorption intensity. (*B*) Second derivative FTIR spectra of truncated ($WT_{truncated}$) and intact bovine αB-crystallin, together with the single-site mutated truncated ($D107G_{truncated}$) bovine αB-crystallin, demonstrating that the 1604 cm^{-1} absorption band is from the intermolecular hydrogen bonds at the dimeric interface. (*C*) Temperature-dependent IR absorbance of intermolecular hydrogen bonds (1604 cm^{-1}) at the dimeric interface in terms of amplitude of the second derivative spectra. The absorbance is derived from the relative intensity of the second derivative peak at 1604 cm^{-1}, as shown in (*A*), which is defined as intensity difference between the absorbance at 1604 and 1595 cm^{-1} (I_{1604}-I_{1595}, where I_{1595} serves as the background intensity). (*D*) Relationship between equilibrium constant ($K(T)$) for breaking the intermolecular hydrogen bonds (1604 cm^{-1}) at the dimeric interface and heating temperatures. ln $K_{H\text{-}bond}(T)$ versus $1/T$ can be well fitted by a straight line at temperatures of 37–67°C, suggesting a continuous disruption of hydrogen bonds at the dimeric interface. (*E* and *F*) IR absorption spectra (*E*) and the corresponding second derivative (*F*) of the three major SVD-resolved species for component 1–3 during the heating process at temperatures of 25–64°C. (*G*) SVD-resolved temperature-dependent population curves for the three components in (*E*) and (*F*). M_{total} represents the total amount of the monomers in solution. Sub_{outer} and Sub_{inner} represent the outermost and inner layer subunits, respectively. (*H*) Linear correlation between the SVD-resolved population of component 2 and the proportion of disrupted hydrogen bonds at the dimeric interface as derived from (*C*). (*I*) The sequential structural transition for the α-crystallin oligomer at elevated temperatures in parallel to the three species-associated components resolved by SVD. Three different colors also represent three resolved species-associated IR spectra, while the corresponding numbers of the colored spheres represent the relative populations.

as-acquired IR spectra can be decomposed into three species-associated spectra. The three SVD-resolved species-associated IR absorption spectra are shown in Fig. 3 *E*, which leads to a fitting residual in optical density within ±0.2‰ (Fig. S7 *B*), and the second derivatives of the corresponding species-associated spectra are presented in Fig. 3

Please cite this article in press as: Li et al., The mechanism for thermal-enhanced chaperone-like activity of α-crystallin against UV irradiation-induced aggregation of γD-crystallin, Biophysical Journal (2022), https://doi.org/10.1016/j.bpj.2022.05.032

F. Thermal titration curves in terms of population are shown in Fig. 3 *G*.

As shown in Fig. 3 *F*, the most hydrophobic β-sheets (component 1) with typical wavenumbers at peaks of 1629 and 1686 cm^{-1} are all blue shifted more than those of the other two spectral components, having the highest portion (86%) of the total population at 25°C (Fig. 3 *G*). This finding suggests that most of the secondary structures in the subunits constituting the bovine α-crystallin oligomer are in the most hydrophobic state, and this population is temperature independent up to 43°C (Fig. 3 *G*), suggesting that it represents the inner subunits of the oligomer. At a higher temperature, above 43°C, the inner subunits (component 1) begin to be converted partially into intermediate hydrophobic β-sheets (component 2), and it should be noted that the population of component 2 is zero at 25°C (Fig. 3 *G*). Meanwhile, the most hydrophilic β-sheets (component 3) has a population of 14% at 25°C, and these β-sheets are continuously converted to the intermediate hydrophobic β-sheets (component 2) as temperature increases to 55°C, then its population begin to increase when the temperature is further elevated (Fig. 3 *G*). Therefore, at RT, only components 1 and 3 exist in solution. If we assume a negligible protein concentration of the dissociated subunits in solution at RT, then SVD analysis clearly indicates that the oligomer consists of two kinds of β-sheet structures, i.e., the most hydrophobic and the most hydrophilic units. Physically, they correspond to the inner hydrophobic and the outer solvent-exposed layers, respectively, if we consider the quaternary structure of the oligomer as a sphere (13). Therefore, component 2 with intermediate hydrophobicity would come from the thermal-induced dissociation of the outer layer in the oligomer at temperatures from RT to 55°C, and the dissociation of the inner layer occurs at a temperature range from 43 to 64°C (Fig. 3 *G*), which is well correlated to the endothermic transition with a respective T_m of 45°C, as revealed by high-resolution calorimetry analysis of bovine α-crystallin (70). Accordingly, component 2 corresponds to the dissociated subunits in solution. Fig. 3 *H* plots the proportion of the disrupted hydrogen bonds at the dimeric interface versus the population of component 2, which leads to a linear correlation, and this result gives a further support for the above assignment. Importantly, the increased population of the outermost layer at temperatures above 55°C strongly suggests the reassembly of the subunits back to the dissociated oligomers at a higher temperature. We noted that Ryazantsev et al. used DLS and analytical ultracentrifugation to measure the size and MW of bovine α-crystallin at temperatures of 7, 25, and 37°C. Their results shows that, when temperature increases, the oligomer has a smaller size accompanied with a loss in MW (13). Explicitly, at 37°C the thermal-induced mass loss is 8.7%, while the curve of component 3 in Fig. 3 *G* gives a mass loss of 7.4% at 37°C. Therefore our result can be corroborated by the orthogonal measurement of analytical ultracentrifugation. Based on the oligomeric structure of α-crystallin, the SVD-resolved three major species-associated spectra would correspond to the following proposed temperature-induced dissociation process, as shown in Fig. 3 *I*.

The high polydispersity of the α-crystallin oligomer prevents the determination of its quaternary structure resolved by x-ray crystallography, and even the recent cryo-EM structure of bovine α-crystallin has not been able to reveal it (13). Several controversial models have been proposed, e.g., a micelle-like model, a model with a tetrameric arrangement of subunits, a three-layer model, and a bean with tentacles model (71). Interestingly, in the three-layer model, the inner core contains 10–16 αA subunits, and the middle layer consists of up to 24 subunits with a molar ratio of 4 αA:1 αB, and the outer shell was thought to contain up to 24 subunits with equal proportions of αA and αB. Therefore, the percentage of αB increases from the inner core to the outer shell in an order of 0, 20, and 50%. Morris et al. used collision-induced dissociation mass spectrometry to examine the architecture of the polydisperse assemblies of α-crystallin (72). Their results show that αB-crystallin subunits dissociate more readily from the mixed oligomers, suggesting that the αA-crystallin subunits forming a most hydrophobic core within the assembly, with αB-crystallin subunits arranged in more exposed positions in the surface, and the more hydrophobic N-terminal domains for either αA or αB are oriented toward the interior of the oligomer, while the more hydrophilic C-terminal domains are exposed to the surface. Accordingly, our proposed IR spectra-resolved three-component model is consistent to this three-layer model of gradient hydrophobicity with the inner core as the most hydrophobic part. The structural correspondence between the three-component model and the three-layer model would be: component 1 to the inner core plus the middle shell, component 3 to the outer layer.

Mechanism for thermal-enhanced protein protection efficiency involving binding of subunit with substrate

As shown in Fig. 4 *A*, the population of the dissociated subunits from the outer layer (M_{outer}) can be evaluated as the difference between the outermost layer subunits (Sub_{outer}) in the oligomer at RT and that at a given temperature, i.e., $M_{outer}(T) = Sub_{outer}(25°C) - Sub_{outer}(T)$, which increases with the temperature rising in the range of 25–55°C, then decreasing as the temperature further increases. This indicates the following process: at a temperature below 55°C, Sub_{outer} dissociates from the oligomer (O_n, n denotes the total number of the subunits) into solution as monomers (M_{outer}); when the temperature exceeds 55°C, the monomers reassemble back to the dissociated oligomer. Since the monomers in solution at a higher temperature could come from the dissociation either from the outermost layer

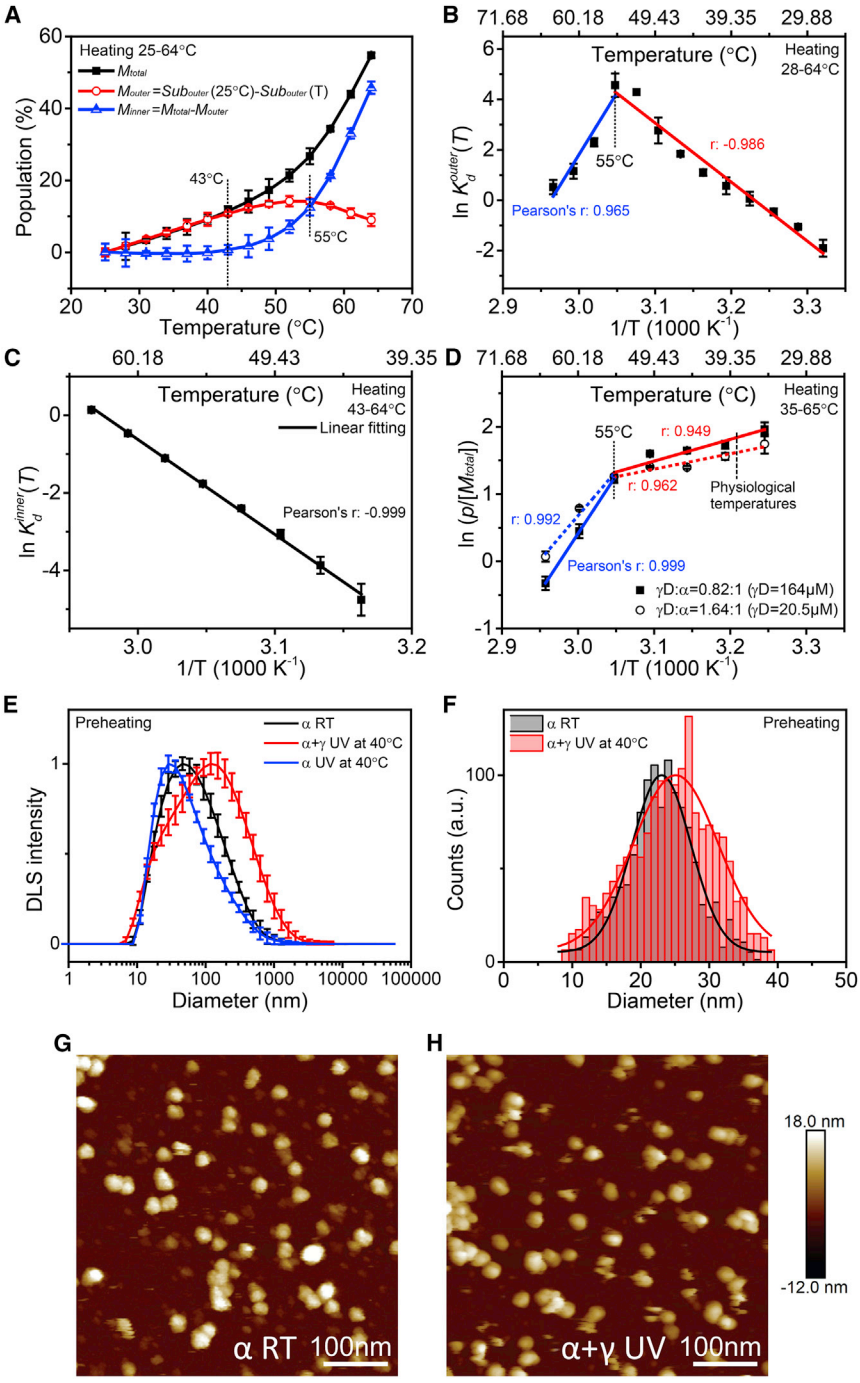

FIGURE 4 Temperature-dependent population of the dissociated subunits, the relationship between the equilibrium constant and heating temperatures, and UV irradiation-induced quaternary structure changes of crystallin oligomer. (*A*) Population of the dissociated subunits from the outer and inner layers of the oligomer. The population of component 2 in Fig. 3 *G* represents the total amount of the dissociated monomers (M_{total}), and the amount of the dissociated monomers (M_{outer}) is derived from the outermost layer subunits (Sub_{outer}) in Fig. 3 *G*. The amount of the dissociated monomers from the inner layer of the oligomer (M_{inner}) is evaluated as the difference between M_{total} and M_{outer}. (*B* and *C*) Correlations between ln $K_d(T)$ and $1/T$ for the subunit dissociation from the outer (*B*) and inner (*C*) layers of the oligomer. K_d denotes the corresponding equilibrium constant. The straight lines are linear fitting lines. (*D*) Correlations between ln (p/[M_{total}]) and $1/T$ in the presence of photodamaged γD-crystallin at the indicated protein concentrations. The relationship can be fitted by two straight lines with a transition temperature of 55°C, similar to the dissociation of the subunits from the outer layer of the oligomer in (*B*). p represents the protein protection efficiency. (*E* and *F*) The average size distribution of α-crystallin and αγ-oligomer upon UV-325 nm exposure as revealed by DLS (*E*) and AFM (*F*) measurements. The photodamaged αγ-oligomer was produced at 40°C. Preheated oligomers were detected at RT with 45 measurements for calculations in DLS. (*G* and *H*) AFM images of α-crystallin without UV irradiation (*G*) and photodamaged αγ-oligomer upon UV-325 nm exposure (*H*). AFM images were constructed using Nikon NIS-Elements AR software.

subunits or the inner layer subunits, their dissociated counterpart monomers in solution are denoted as M_{outer} and M_{inner}, respectively, hence the total amount of the monomers in solution would be $M_{total} = M_{outer} + M_{inner}$. Fig. 4 *A* also plots the population of the total dissociated monomer (M_{total}, i.e., the population of component 2 in Fig. 3 *G*) for comparison, which reveals that the subunits in solution almost completely come from the outermost layer of the oligomer when the temperature is below 43°C, while the contribution from the inner layer becomes significant at a higher temperature. The difference between the population of component 2 (M_{total}) and M_{outer} is given in Fig. 4 *A*, which presents the amount of the dissociated subunits from the inner layer of the oligomer (M_{inner}). This is consistent with the proposed transition for the dissociation-reassociation of the subunits from α-crystallin oligomer (Fig. 3 *I*).

In the previously proposed mechanism for α-crystallin preventing the aggregation of γ-crystallin, it is assumed that, in the first phase of aggregation, γ-crystallin forms dimers and higher-order oligomers (31) unless α-crystallin

Please cite this article in press as: Li et al., The mechanism for thermal-enhanced chaperone-like activity of α-crystallin against UV irradiation-induced aggregation of γD-crystallin, Biophysical Journal (2022), https://doi.org/10.1016/j.bpj.2022.05.032

sequesters γ-crystallin by forming an αγ-complex. Furthermore, it has been demonstrated that a single α-crystallin oligomer can bind up to seven substrate units (73). Since α-crystallin is a member of the sHsp family, its mechanism of protection would follow the general mechanism for sHsps. Haslbeck et al. (74) suggested that, for yeast Hsp26, protein dissociation is a prerequisite for the chaperone function and the Hsp26 dimer may act as the primary substrate binding species, followed by reassembly into a larger complex with the substrate. The temperature-dependent dissociation of the large storage form of Hsp26 into smaller, active species and the subsequent reassociation to a defined large chaperone-substrate complex represents a novel mechanism for the functional activation of a molecular chaperone (74). Therefore, in the presence of the denatured γD-crystallin monomer, the following equilibria would exist:

(1) Dissociation and reassociation between the oligomers (O_n, O_{n-1}) and dissociated subunits as the monomers in solution (M_{total}). K_d represents the equilibrium constant for the subunit dissociation.

$$O_n \overset{K_d}{\rightleftharpoons} O_{n-1} + M_{total}, K_d = \frac{[O_{n-1}][M_{total}]}{[O_n]}$$

(2) Binding of the substrate (γ) with the monomers in solution. K_b represents the equilibrium constant for the substrate binding.

$$M_{total} + \gamma \overset{K_b}{\rightleftharpoons} M^{\gamma}_{total}, K_b = \frac{[M^{\gamma}_{total}]}{[M_{total}][\gamma]},$$

where M^{γ}_{total} is the complex formed by binding of the denatured γ-crystallin to the α-crystallin monomers in solution, i.e., the αγ-complex.

(3) Reassociation and dissociation between the oligomer (O_{n-1}) and αγ-complex bound oligomer (O^{γ}_n). K^{γ}_b represents the equilibrium constant for the reassociation of the αγ-complex.

$$O_{n-1} + M^{\gamma}_{total} \overset{K^{\gamma}_b}{\rightleftharpoons} O^{\gamma}_n, K^{\gamma}_b = \frac{[O^{\gamma}_n]}{[O_{n-1}][M^{\gamma}_{total}]}$$

Obviously, the protein protection efficiency (p) is proportional to the amount of αγ-oligomers, i.e., $p = c\sum_n [O^{\gamma}_n]$, where c is a constant, and $[O^{\gamma}_n] = K^{\gamma}_b K_b [\gamma][O_{n-1}][M_{total}]$. Since the total amount of oligomers with different numbers of subunits is almost independent on the varied temperatures, we take $\sum_n [O_n]$ as a value of c_0 at RT. Thus, $In\frac{p}{[M_{total}]} = -\frac{\Delta H}{RT} + A$, where $\Delta H = \Delta H^{\gamma}_b + \Delta H_b$ and A is a constant. For the dissociation of the outer layer in the oligomer, $K^{outer}_d(T) = \frac{[M_{outer}(T)]}{[Sub_{outer}(T)]} = \frac{[Sub_{outer}(25°C)] - [Sub_{outer}(T)]}{[Sub_{outer}(T)]}$. Fig. 4 *B* plots $In\, K^{outer}_d(T)$ against $1/T$, which gives rise to two straight lines with different slopes, corresponding to an enthalpy difference of $\Delta H^{outer}_d = 46.6 \pm 2.8$ kcal mol^{-1} and an entropy difference of $\Delta S^{outer}_d = 150.4 \pm 8.9$ cal mol^{-1}K^{-1} in a temperature range of 28–55°C, and $\Delta H^{outer}_d = -97.4 \pm 18.6$ kcal mol^{-1} and $\Delta S^{outer}_d = -288.7 \pm 56.0$ cal mol^{-1}K^{-1} in a temperature range of 55–64°C. The results indicate that the dissociation of the outer layer subunits in the oligomer into solution at a temperature range from 28 to 55°C is endothermic or thermally activated and, above 55°C, such a dissociation becomes exothermic. This might be caused by the reassociation of the dissociated subunits back to the oligomer since this process starts approximately at a temperature of 55°C judged from the turning point of population curve of component 3 in Fig. 3 *G* and a negative entropy change. Similarly, a plot of M_{inner} against $1/T$ in at temperatures of 43–64°C leads to a straight line (Fig. 4 *C*), giving rise to an enthalpy difference of $\Delta H^{inner}_d = 48.6 \pm 0.9$ kcal mol^{-1} and an entropy difference of $\Delta S^{inner}_d = 144.5 \pm 2.8$ cal mol^{-1}K^{-1}, where M_{inner} is derived from the inner subunits (Sub_{inner}), i.e., component 1, $K^{inner}_d(T) = \frac{[M_{inner}(T)]}{[Sub_{inner}(T)]} = \frac{[M_{total(T)}] - [M_{outer}(T)]}{[Sub_{inner}(T)]}$. This indicates that the dissociation of the inner subunits from the oligomer is also endothermic. Then we plot $In\frac{p}{[M_{total}]}$ against $1/T$ for two different γD-crystallin concentrations of 164 and 20.5 μM, respectively (Fig. 4 *D*). Both lead to two straight lines with different slopes in a low and high temperature region, corresponding to their respective enthalpy differences of -6.4 ± 1.2 (γ:α molar ratio of 0.82:1) and -4.5 ± 0.7 kcal mol^{-1} (γ:α molar ratio of 1.64:1) at a temperature of 35–55°C, and -34.3 ± 0.3 (γ:α molar ratio of 0.82:1) and -26.2 ± 3.4 kcal mol^{-1} (γ:α molar ratio of 1.64:1) in a temperature of 55–65°C, which indicates that the protein binding and reassociation is exothermic ($\Delta H^{\gamma}_b + \Delta H_b < 0$). Therefore, once α-crystallin is dissociated, the chaperone function against UV irradiation-induced aggregation of γD-crystallin would occur probably spontaneously if we the neglect the contribution from the entropy difference in such a dynamical equilibrium system. Apparently, the subunits in solution disscociated from the outermost layer (M_{outer}) are the most effective for the thermal-induced chaperone activity at temperatures of 25–43°C, since the contribution from the inner layer (M_{inner}) is negligible at a lower temperature (Fig. 4 *A*) and the substrate binding is exothermic (Fig. 4 *D*).

To verify the assumption that the αγ-complex reassociates with the partially dissociated α-crystallin oligomer, the sizes of the preheated α-crystallin only, α-crystallin with UV-325 nm irradiation, and α-crystallin in the presence of γD-crystallin with UV-325 nm irradiation have been inspected using DLS, and the results are presented in Fig. 4 *E*. In contrast, the size of γD-crystallin is too small to give a detectable DLS signal within our instrumental limit. The results show that the hydrodynamic size for the preheated α-crystallin of ∼40 nm increases to ∼125 nm for

Please cite this article in press as: Li et al., The mechanism for thermal-enhanced chaperone-like activity of α-crystallin against UV irradiation-induced aggregation of γD-crystallin, Biophysical Journal (2022), https://doi.org/10.1016/j.bpj.2022.05.032

the preheated αγ-crystallin oligomer, reflecting the reassociation of the denatured γD-crystallin to the partially dissociated α-crystallin oligomer. Meanwhile, the hydrodynamic size change in UV irradiated α-crystallin oligomer shows a tendency to decrease, indicating that the αγ-oligomer size expansion is not caused by the aggregation of α-crystallin but the binding of γD-crystallin to α-crystallin. Furthermore, such a size expansion is more accurately reflected by the AFM measurement, which reveals that the average size changes from 22 to 26 nm (Fig. 4, *F–H*).

Thermal-induced breaking of hydrogen bonds at the dimeric interface revealed by T-jump time-resolved IR spectra

To probe the thermal-induced transient structural changes of bovine α-crystallin, we acquired the transient IR absorbance difference spectra in the amide I′ band and recorded the kinetics after a T-jump of 10°C from RT to 35°C. The increased temperature will first cause dissociation of the outer layer subunits by breaking the hydrogen bonds at the dimeric interface, then lead to the dissociation of the subunits from the oligomer. The T-jump time-resolved IR absorbance difference spectra at two different pH are shown in Fig. 5 *A*, which reveals that the appearance of the absorption peaks at 1656 and 1669 cm^{-1} is accompanied by bleaching peaks at 1620 and 1648 cm^{-1}. This result indicates that the transient formation of loop structures (1656 cm^{-1}) and β-turns (1669 cm^{-1}) from hydrophilic β-sheets (1620 cm^{-1}) and random coils (1648 cm^{-1}) (spectral assignments with corresponding references are provided in Table S1). All the spectral features are similar for the samples under two different pH conditions except that α-crystallin at pH 5 is more susceptible to thermal-induced dissociation revealed by a larger transient bleaching signal. Typical kinetics of antiparallel β-sheets at the lower frequency at 1620 cm^{-1}, random coils at 1648 cm^{-1}, and intermolecular hydrogen bonds at the dimeric interface at 1602 cm^{-1} are depicted in Fig. 5, *B*, *C*, and *E*, together with the respective fitted kinetics (*dotted lines*). The protein structures of both αA-crystallin (6T1R) (55) and αB-crystallin (2YGD) (57) show that there are some unordered

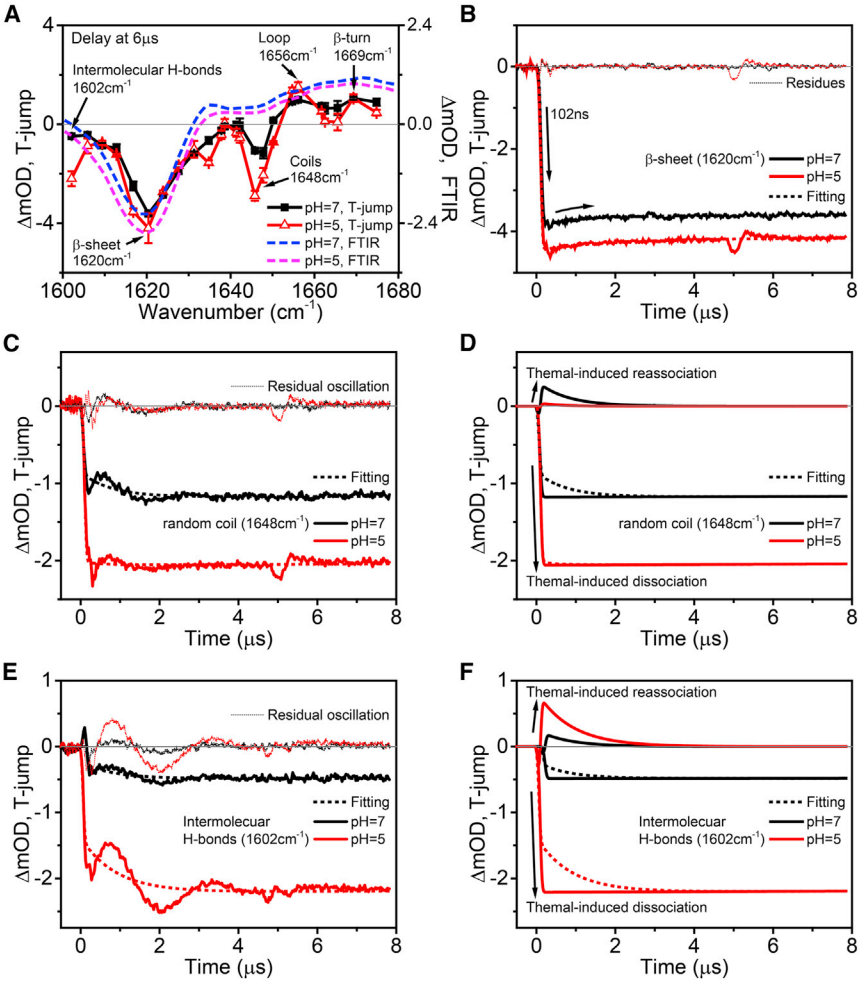

FIGURE 5 T-jump time-resolved IR absorbance difference spectra of bovine α-crystallin and typical kinetics for structural changes of hydrophilic β-sheets, random coils, and intermolecular hydrogen bonds. (*A*) Time-resolved IR absorption difference (ΔOD) spectra of bovine α-crystallin at a T-jump value of 10°C from RT delayed by 6 μs with respect to the heating laser pulse. (*B*, *C*, and *E*) Kinetics for structural changes of (*B*) hydrophilic β-sheets (1620 cm^{-1}), (*C*) random coils (1648 cm^{-1}), and (*E*) the intermolecular hydrogen bonds at the dimeric interface (1602 cm^{-1}) after a T-jump of $\Delta T = 10$°C at two different pH values. The fitted kinetics are shown as dotted lines, and the damped oscillation in the fitting residual for random coils and the intermolecular hydrogen bonds might be attributed to a heat propagation at the interface to the sample (83,84). (*D* and *F*) Fitting of T-jump transient kinetics for IR absorbance of (*D*) random coils (1648 cm^{-1}) and (*F*) the intermolecular hydrogen bonds at the dimeric interface (1602 cm^{-1}). The fitting kinetics in (*C* and *E*) can be decomposed into two processes, corresponding to the thermal-induced dissociation and reassociation.

Please cite this article in press as: Li et al., The mechanism for thermal-enhanced chaperone-like activity of α-crystallin against UV irradiation-induced aggregation of γD-crystallin, Biophysical Journal (2022), https://doi.org/10.1016/j.bpj.2022.05.032

structural segments at both N- and C-termini, which connect the β-strands. They can be random coil structures absorbing around 1648 cm^{-1}. When unfolded, a significant structural change occurs at the dimeric interface as demonstrated by a significant decrease in the β-strand absorption at 1620 cm^{-1}. This is accompanied by a decrease in random coil absorption at 1648 cm^{-1} and an increase in the absorption for loop structure at 1656 cm^{-1}. This fact indicates that the random coil structures linking the β-strands at the dimeric interface change to the loop structures during thermal-induced unfolding.

Further analysis shows that the kinetics at 1620 cm^{-1} can be fitted by a respective fast bleaching phase with a time constant of 102 ns, followed by a slow absorption phase (Fig. 5 *B*). While the kinetics at 1648 and 1602 cm^{-1} (Fig. 5, *C* and *E*) can be fitted by a fast absorption decay followed by a slow bleaching component (Fig. 5, *D* and *F*). The two kinetic components can be interpreted by a dynamical equilibrium as a response of the unfolding (k_+) and refolding (k_-) of protein secondary structures (75) to a T-jump as follow:

$$Sub_{outer}^{folded} \underset{k_-}{\overset{k_+}{\rightleftharpoons}} Sub_{outer}^{unfolded}$$

For the antiparallel β-sheets absorbing at 1620 cm^{-1}, the forward reaction, i.e., thermal-induced unfolding process, is dominant over the reverse process (Fig. 5 *B*). For random coils at 1648 cm^{-1} and the intermolecular hydrogen bonds at the dimeric interface at 1602 cm^{-1}, both the forward (bleaching) and backward (absorption) occur almost simultaneously, suggesting that a dynamical equilibrium exists (Fig. 5, *D* and *F*), and the sum of the individual beaching and absorption kinetics results in the fitted kinetics (Fig. 5, *C–F*). This suggests that, when the temperature jumps from RT to 35°C, the instantly formed folded structure (indicated as absorbance) becomes unfolded with an exponential decay and, after several μs, it reaches a new equilibrium at 35°C (Fig. 5, *C* and *E*). Therefore, our T-jump results clearly indicate that part of random coils and the intermolecular hydrogen bonds at the dimeric interface are in a dynamical equilibrium with their unfolded counter parts, consistent with the fact that the oligomer is in a dynamical equilibrium with the subunits in solution (13,76).

DISCUSSION

Thermal-enhanced chaperone-like activity of α-crystallin against UV irradiation-induced aggregation of γ-crystallin has been confirmed by a number of groups (38–40), and it is believed that α- and γ-crystallins could form a stable complex via hydrophobic interaction (37,77–79), but the detailed mechanism involving quaternary, tertiary, and secondary structures of the protein remains to be further explored. In this work, we first investigated the photodamaged products of γD-crystallin in the presence of α-crystallin under UV-325 nm irradiation using LC-MS, and attributed the truncated peptides with a reduced MW to the backbone cleavage at Ala158 in γD-crystallin. A possible mechanism for this bond cleavage can be that UV light absorption by Trp156 leads to the formation of indolyl radicals in the presence of oxygen, which attack the C_α-N bond at Ala158, giving rise to a truncation of a short peptide with 16 residues at the C-terminus from γD-crystallin (Fig. 6 *A*). Meanwhile, UV-325 nm irradiation-induced aggregation of unfolded γD-crystallin without α-crystallin generates a strong coupling between tryptophan residues of adjacent γD-crystallin molecules, which contributes to the dissipation of the excited energy via tryptophan quenching without initiating further bond cleavage reaction (80). Then we reproduced the thermal-enhanced chaperone-like activity of bovine α-crystallin against UV-photodamaged human γD-crystallin (Fig. 2 *A*) and attributed such a protection to the binding of the αγ-complex to the partially dissociated α-crystallin oligomers. After preheat treatment, the retained exposed hydrophobic surface in α-crystallin was detected at RT using a hydrophobic fluorescence molecular probe (bis-ANS), and the fluorescence intensity of protein-bound bis-ANS was linearly correlated to the protein protection efficiency against aggregation of denatured γD-crystallin and insulin (Fig. 2 *D*). This result unambiguously demonstrates that the interaction between α-crystallin and the substrate proteins occurs at the thermal-induced exposed hydrophobic surface. We also employed an IR fingerprint at 1604 cm^{-1} as a probe for the intermolecular hydrogen bonds at the dimeric interface, and the enthalpy and entropy changes determined in the temperature range from 37 to 67°C are 22.6 ± 0.9 kcal mol^{-1} and 64.5 ± 2.8 cal mol^{-1} K^{-1} (Fig. 3 *D*). It has been shown that a charged intermolecular hydrogen bond contributes up to 4.7 kcal mol^{-1} in binding energy (81); therefore, it can be suggested that there are approximately four to five hydrogen bonds breaking at the dimeric interface as temperature increases.

Bovine α-crystallin is an oligomer with 35–50 subunits in a dynamic equilibrium through the breaking and formation of hydrogen bonds at the dimeric interface (13). Using SVD analysis, the temperature-dependent IR absorption spectra can be resolved into three species-associated components (Fig. 3, *E* and *I*). The most hydrophobic component (component 1) with a population of 86% at RT corresponds to the subunits in the inner layer. The intermediate hydrophobic component (component 2) is derived from the dissociated subunits in solution, and its temperature-dependent population is linearly correlated to the corresponding amount of broken hydrogen bonds at the dimeric interface (Fig. 3 *H*). While the most hydrophilic component (component 3) with a population of 14% at RT represents the subunits in the outer layer of the oligomer. These outer layer subunits start to dissociate at RT, as indicated by a

Please cite this article in press as: Li et al., The mechanism for thermal-enhanced chaperone-like activity of α-crystallin against UV irradiation-induced aggregation of γD-crystallin, Biophysical Journal (2022), https://doi.org/10.1016/j.bpj.2022.05.032

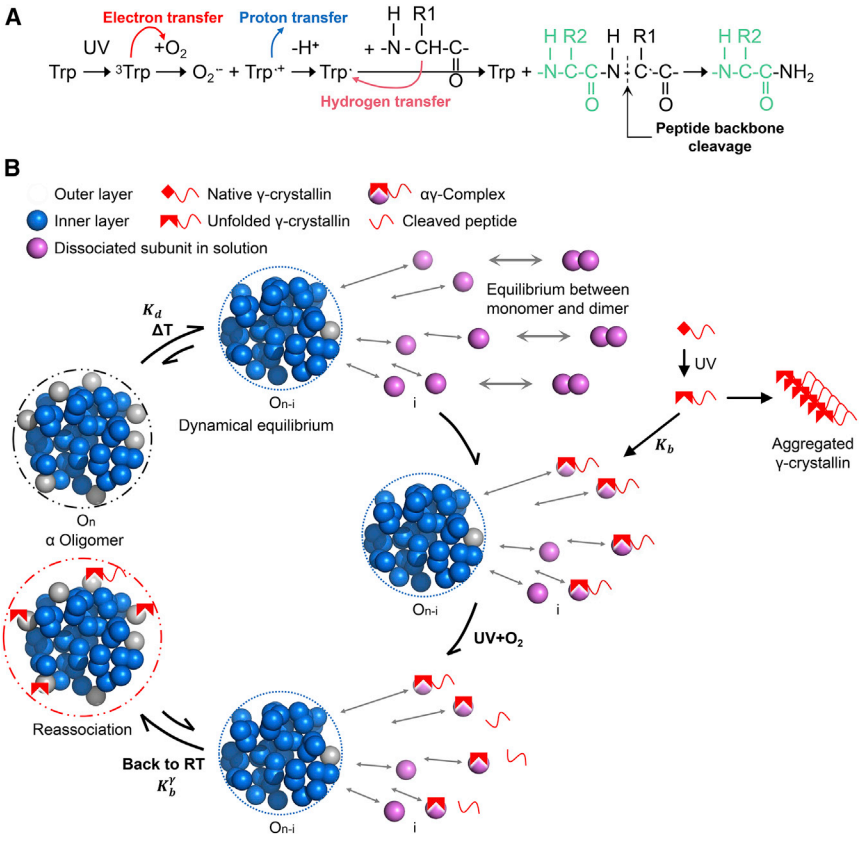

FIGURE 6 Pathway for the photolytic cleavage of peptide backbone and mechanism for the thermal-enhanced chaperone-like activity of bovine α-crystallin. (*A*) A possible photolytic pathway for UV absorption of tryptophan (Trp) inducing peptide bond cleavage in γD-crystallin (36). (*B*) Mechanism for the thermal-enhanced chaperone-like activity of bovine α-crystallin involving the formation of a stable complex between the chaperone and substrate γD-crystallin proteins. This mechanism occurs at temperatures of 25–43°C, and the substrate (unfolded γD-crystallin) binds to the dissociated subunits in solution from the outer layer of the α-crystallin oligomer. K_d represents the equilibrium constant for the subunit dissociation. K_b represents the equilibrium constant for the substrate binding. K_b^γ represents the equilibrium constant for the reassociation of the αγ-complex.

continuous decrease in the population as the temperature increases from RT to 55°C. When temperature is above 55°C, the reassociation of the subunits back to the oligomer overwhelms the dissociation (Fig. 3 *G*). The enthalpy change for the dissociation of the outer layer subunits is 46.6 ± 2.8 kcal mol^{-1} at temperatures of 28–55°C, and −97.4 ± 18.6 kcal mol^{-1} in a temperature range of 55–64°C (Fig. 4 *B*), which indicates that the oligomer dissociation is predominant and endothermic at temperatures below 55°C, and the reassociation occurs at temperatures above 55°C (Fig. 3 *G*, population curve of outer layer subunits), which becomes exothermic. This might be caused by the reassociation of the dissociated subunits back to the oligomer since this process starts approximately at a temperature of 55°C. The dissociation energy of 46.6 ± 2.8 kcal mol^{-1} in the lower temperature region is significantly higher than the energy necessary for breaking hydrogen bonds at the dimeric interface of 22.6 ± 0.9 kcal mol^{-1}, and this difference suggests an additional hydrophobic interaction energy of 24.0 kcal mol^{-1} for the oligomerization of subunits. Accordingly, the enthalpy difference for the dissociation of the inner layer subunits can be determined as 48.6 ± 0.9 kcal mol^{-1} (Fig. 4 *C*).

In the presence of UV irradiation-denatured γD-crystallin, the dissociated subunits in solution bind the denatured γD-crystallin via hydrophobic interaction, and the reassociation of dissociated subunits to the αγ-complex has an enthalpy difference of −6.4 ± 1.2 (γ:α molar ratio of 0.82:1) and −4.5 ± 0.7 kcal mol^{-1} (γ:α molar ratio of 1.64:1) at temperatures below 55°C, and −34.3 ± 0.3 (γ:α molar ratio of 0.82:1) and −26.2 ± 3.4 kcal mol^{-1} (γ:α molar ratio of 1.64:1) in a temperature range of 55–65°C for two different γD-crystallin concentrations of 164 and 20.5 μM, respectively. An important thermodynamic feature is that the reassociation of dissociated subunits to the αγ-complex is exothermic, which can be considered as a spontaneous process. We further confirmed the binding of UV-325 nm irradiation-denatured γD-crystallin to the α-crystallin oligomer by inspecting the corresponding geometrical size expansion via AFM and DLS analysis. AFM shows an average size change from 22 to 26 nm at a preheat temperature of 40°C (Fig. 4 *F*).

Finally, the disruption of hydrogen bonds at the dimeric interface (1602 cm^{-1}) has been further verified by T-jump time-resolved IR absorbance difference spectra, with a $\Delta T = 10$°C. The response of the interfacial hydrogen bonds and random coils to a T-jump reveals a dynamical equilibrium of these loose structures, which is consistent with the dynamical equilibrium between the dissociated subunits and oligomers in solution (13), and the subunit dissociation from the oligomer is further enhanced by the increased acidity (Fig. 5, *B*, *C*, and *E*). Based on the available facts and our current results, a mechanism for thermal-enhanced

Please cite this article in press as: Li et al., The mechanism for thermal-enhanced chaperone-like activity of α-crystallin against UV irradiation-induced aggregation of γD-crystallin, Biophysical Journal (2022), https://doi.org/10.1016/j.bpj.2022.05.032

chaperone-like activity of bovine α-crystallin against UV irradiation-denatured γD-crystallin is proposed, as summarized in Fig. 6 *B*, in which an equilibrium between the monomer and dimer of α-crystallin in solution is ensured (82).

CONCLUSIONS

In this study, UV-325 nm irradiation-yielded products of γD-crystallin in the presence and absence of α-crystallin were analyzed by LC-MS measurement. Our results reveal that, in the presence of α-crystallin, αγ-crystallin oligomers are formed, while γD-crystallin undergoes a bond cleavage at Ala158, leading to a C-terminal truncation of a hydrophilic short peptide chain with 16 residues. Meanwhile, γD-crystallin in the absence of α-crystallin only undergoes aggregation without bond cleavage. The temperature-dependent chaperone-like activity of bovine α-crystallin against UV irradiation-induced aggregation of γD-crystallin has been investigated, and the results are consistent with previous reports, i.e., the chaperone-like activity of α-crystallin is thermal activated. FTIR absorption spectra and T-jump time-resolved IR absorbance difference spectra were employed to characterize the thermal-induced secondary structure changes of bovine α-crystallin, which reveal that the subunit dissociation from the oligomer involves the breaking of hydrogen bonds at the dimeric interface. Using SVD analysis of IR absorption spectra, three types of species-associated IR spectra were resolved, i.e., those for the most hydrophobic species in the inner layer, the intermediate hydrophobic species with the dissociated subunits in solution, and the most hydrophilic species in the outer layer. Especially, the dissociated subunits in solution are exclusively converted from the most hydrophilic subunits in the outer layer at temperatures of 25–43°C, and from both the most hydrophilic and hydrophobic species at higher temperatures up to 55°C. It is the dissociated subunits in solution that bind the UV irradiation-induced unfolded γD-crystallin to form the αγ-complex. In the presence of photodamaged γD-crystallin, the reassembly of the αγ-complex to the partially dissociated oligomer is exothermic and spontaneous, which contributes to the effective chaperone-like activity of the α-crystallin oligomers against the aggregation of UV irradiation-denatured γD-crystallin. The binding of γD-crystallin to the α-crystallin oligomer has been confirmed by the AFM and DLS measurements. In addition, the fluorescence of protein-bound bis-ANS further confirms that the interaction between the preheated α-crystallin and substrate proteins occurs at the thermal-induced exposed hydrophobic surface based on the linear correlation between the fluorescence intensity and the protein protection efficiency against aggregation of denatured γD-crystallin and insulin, and this result also suggests a mechanism for bovine α-crystallin to keep a balance between its water solubility (hydrophilic surface exposed) and chaperone-like activity (hydrophobic surface exposed). Obviously, the chaperone function of bovine α-crystallin protecting UV irradiation-induced aggregation of human γD-crystallin is at an expense of a loss in a hydrophilic 16-residue short peptide chain.

SUPPORTING MATERIAL

Supporting material can be found online at https://doi.org/10.1016/j.bpj.2022.05.032.

AUTHOR CONTRIBUTIONS

H.L. carried out the experiments, collected the data, and performed analyses with help from Y.-y.Y. on the measurement of chaperone-like activity, M.-x.R. on fluorescence measurements and protein irradiation, F.J. on AFM measurements and analysis, H.-l.C. on the programming of SVD analysis system, and J.l.G. on the guidance in LC-MS and DLS measurements. H.L. prepared all figures. Y.-x.W and H.L. wrote and edited the manuscript. Y.-x.W. and Y.-z.B. supervised and coordinated the whole project.

DECLARATION OF INTERESTS

The authors declare no competing interests.

ACKNOWLEDGMENTS

Y.-x.W. and H.L. thank Professor Yong-bin Yan and Doctor Yibo Xi for the Human γD-crystallin sample, Doctor Deyong Li on the T-jump time-resolved IR instrumentation setup, Doctor Haoyi Wang for the programming of the data acquisition system, Doctor Haidi Yin from the Mass Spectrometry Core Facility of Shenzhen Bay Laboratory for mass spectrometry analysis, and Professor Qin Peng for the help in using Nikon NIS-Elements AR software.

This work was supported by the National Natural Science Foundation of China (nos. 21433014, 11721404, and 21173012) and the Chinese Academy of Sciences (QYZDJ-SSW-SYS017 and YJKYYQ20170046).

REFERENCES

1. Moreau, K. L., and J. A. King. 2012. Protein misfolding and aggregation in cataract disease and prospects for prevention. *Trends Mol. Med.* 18:273–282. https://doi.org/10.1016/j.molmed.2012.03.005.
2. De Jong, W. W. 1981. Evolution of lens and crystallins. *In* Molecular and Cellular Biology of the Eye Lens. H. Bloemendal, ed John Wiley and Sons Inc., New York, pp. 221–278.
3. Horwitz, J. 2003. Alpha-crystallin. *Exp. Eye Res.* 76:145–153. https://doi.org/10.1016/s0014-4835(02)00278-6.
4. Horwitz, J. 2009. Alpha crystallin: the quest for a homogeneous quaternary structure. *Exp. Eye Res.* 88:190–194. https://doi.org/10.1016/j.exer.2008.07.007.
5. Das, K. P., L. P. Choo-Smith, …, W. K. Surewicz. 1999. Insight into the secondary structure of non-native proteins bound to a molecular chaperone α-crystallin. *J. Biol. Chem.* 274:33209–33212. https://doi.org/10.1074/jbc.274.47.33209.
6. Sprague-Piercy, M., E. Wong, …, R. W. Martin. 2019. Human αB-crystallin discriminates between aggregation-prone and function-preserving variants of a client protein. *Biochim. Biophys. Acta Gen. Subj.* 1864:129502.

7. Abgar, S., N. Yevlampieva, …, J. Clauwaert. 2000. Chaperone-like activity of bovine lens α-crystallin in the presence of dithiothreitol-destabilized proteins: characterization of the formed complexes. *Biochem. Bioph. Res. Co.* 276:619–625. https://doi.org/10.1006/bbrc.2000.3518.

8. Horwitz, J. 1992. Alpha-crystallin can function as a molecular chaperone. *Proc. Natl. Acad. Sci. U.S.A.* 89:10449–10453. https://doi.org/10.1073/pnas.89.21.10449.

9. Haslbeck, M., J. Peschek, …, S. Weinkauf. 2016. Structure and function of α-crystallins: traversing from in vitro to in vivo. *Biochim. Biophys. Acta Gen. Subj.* 1860:149–166. https://doi.org/10.1016/j.bbagen.2015.06.008.

10. Muranov, K. O., N. B. Poliansky, …, M. A. Ostrovsky. 2019. The mechanism of the interaction of α-crystallin and UV-damaged βL-crystallin. *Int. J. Biol. Macromol.* 140:736–748. https://doi.org/10.1016/j.ijbiomac.2019.08.178.

11. Bloemendal, H., W. de Jong, …, A. Tardieu. 2004. Ageing and vision: structure, stability and function of lens crystallins. *Prog. Biophys. Mol. Biol.* 86:407–485. https://doi.org/10.1016/j.pbiomolbio.2003.11.012.

12. Spector, A., L. K. Li, …, T. Freund. 1971. α-Crystallin. The isolation and characterization of distinct macromolecular fractions. *Biochem. J.* 124:337–343. https://doi.org/10.1042/bj1240337.

13. Ryazantsev, S. N., N. B. Poliansky, …, K. O. Muranov. 2018. 3D structure of the native α-crystallin from bovine eye lens. *Int. J. Biol. Macromol.* 117:1289–1298. https://doi.org/10.1016/j.ijbiomac.2018.06.004.

14. Bova, M. P., H. S. McHaourab, …, B. K. K. Fung. 2000. Subunit exchange of small heat shock proteins. *J. Biol. Chem.* 275:1035–1042. https://doi.org/10.1074/jbc.275.2.1035.

15. Narberhaus, F. 2002. α-Crystallin-type heat shock proteins: socializing minichaperones in the context of a multichaperone network. *Microbiol. Mol. Biol. Rev.* 66:64–93. https://doi.org/10.1128/mmbr.66.1.64-93.2002.

16. Stromer, T., E. Fischer, …, J. Buchner. 2004. Analysis of the regulation of the molecular chaperone Hsp26 by temperature-induced dissociation. *J. Biol. Chem.* 279:11222–11228. https://doi.org/10.1074/jbc.m310149200.

17. Treweek, T. M., A. Rekas, …, J. A. Carver. 2010. A quantitative NMR spectroscopic examination of the flexibility of the C-terminal extensions of the molecular chaperones, αA- and αB-crystallin. *Exp. Eye Res.* 91:691–699. https://doi.org/10.1016/j.exer.2010.08.015.

18. Lindner, R. A., J. A. Carver, …, M. Gaestel. 2000. Mouse Hsp25, a small heat shock protein. *Eur. J. Biochem.* 267:1923–1932. https://doi.org/10.1046/j.1432-1327.2000.01188.x.

19. Phadte, A. S., P. Santhoshkumar, and K. K. Sharma. 2018. Characterization of an N-terminal mutant of αA-crystallin αA-R21Q associated with congenital cataract. *Exp. Eye Res.* 174:185–195. https://doi.org/10.1016/j.exer.2018.05.016.

20. Takata, T., T. Matsubara, …, N. Fujii. 2019. Negative charge at aspartate 151 is important for human lens αA-crystallin stability and chaperone function. *Exp. Eye Res.* 182:10–18. https://doi.org/10.1016/j.exer.2019.02.023.

21. Haslbeck, M., A. Ignatiou, …, J. Buchner. 2004. A domain in the N-terminal part of Hsp26 is essential for chaperone function and oligomerization. *J. Mol. Biol.* 343:445–455. https://doi.org/10.1016/j.jmb.2004.08.048.

22. Plater, M. L., D. Goode, and M. J. C. Crabbe. 1996. Effects of site-directed mutations on the chaperone-like activity of αB-crystallin. *J. Biol. Chem.* 271:28558–28566. https://doi.org/10.1074/jbc.271.45.28558.

23. Jehle, S., B. van Rossum, …, P. Rajagopal. 2009. αB-Crystallin: a hybrid solid-state/solution-state NMR investigation reveals structural aspects of the heterogeneous oligomer. *J. Mol. Biol.* 385:1481–1497. https://doi.org/10.1016/j.jmb.2008.10.097.

24. Slingsby, C., G. J. Wistow, and A. R. Clark. 2013. Evolution of crystallins for a role in the vertebrate eye lens. *Protein Sci.* 22:367–380. https://doi.org/10.1002/pro.2229.

25. Ghosh, J. G., M. R. Estrada, and J. I. Clark. 2005. Interactive domains for chaperone activity in the small heat shock protein, human αB crystallin. *Biochemistry.* 44:14854–14869. https://doi.org/10.1021/bi0503910.

26. Muchowski, P. J., G. J. Wu, …, J. I. Clark. 1999. Site-directed mutations within the core "α-crystallin" domain of the small heat-shock protein, human αB-crystallin, decrease molecular chaperone functions. *J. Mol. Biol.* 289:397–411. https://doi.org/10.1006/jmbi.1999.2759.

27. Sharma, K. K., H. Kaur, and K. Kester. 1997. Functional elements in molecular chaperone alpha-crystallin: identification of binding sites in alpha B-crystallin. *Biochem. Bioph. Res. Co.* 239:217–222. https://doi.org/10.1006/bbrc.1997.7460.

28. Sharma, K. K., G. S. Kumar, …, K. Kester. 1998. Identification of 1, 1'-bi(4-anilino) naphthalene-5, 5'-disulfonic acid binding sequences in alpha-crystallin. *J. Biol. Chem.* 273:15474–15478. https://doi.org/10.1074/jbc.273.25.15474.

29. Basak, A., O. Bateman, …, J. Pande. 2003. High-resolution X-ray crystal structures of human γD crystallin (1.25Å) and the R58H mutant (1.15Å) associated with aculeiform cataract. *J. Mol. Biol.* 328:1137–1147. https://doi.org/10.1016/s0022-2836(03)00375-9.

30. Flaugh, S. L., M. S. Konsinski-Collins, and J. King. 2005. Contributions of hydrophobic domain interface interactions to the folding and stability of human γD-crystallin. *Protein Sci.* 14:569–581. https://doi.org/10.1110/ps.041111405.

31. Serebryany, E., T. Takata, …, J. A. King. 2016. Aggregation of Trp > Glu point mutants of human gamma-D crystallin provides a model for hereditary or UV-induced cataract. *Protein Sci.* 25:1115–1128. https://doi.org/10.1002/pro.2924.

32. Chen, J., P. R. Callis, and J. King. 2009. Mechanism of the very efficient quenching of tryptophan fluorescence in human γD- and γS-crystallins: the γ-crystallin fold may have evolved to protect tryptophan residues from ultraviolet photodamage. *Biochemistry.* 48:3708–3716. https://doi.org/10.1021/bi802177g.

33. Chen, J., S. L. Flaugh, …, J. King. 2006. Mechanism of the highly efficient quenching of tryptophan fluorescence in human γD-crystallin. *Biochemistry.* 45:11552–11563. https://doi.org/10.1021/bi060988v.

34. Xu, J., J. Chen, …, J. R. Knutson. 2009. Femtosecond fluorescence spectra of tryptophan in human gamma-Crystallin mutants: sitedependent ultrafast quenching. *J. Am. Chem. Soc.* 131:16751–16757. https://doi.org/10.1021/ja904857t.

35. Moran, S. D., T. O. Zhang, …, M. T. Zanni. 2013. Amyloid fiber formation in human γD-Crystallin induced by UV-B photodamage. *Biochemistry.* 52:6169–6181. https://doi.org/10.1021/bi4008353.

36. Kerwin, B. A., and R. L. Remmele. 2007. Protect from light: photodegradation and protein biologics. *J. Pharm. Sci.* 96:1468–1479. https://doi.org/10.1002/jps.20815.

37. Sharma, K. K., H. Kaur, …, K. Kester. 1998. Interaction of 1, 1′-bi(4-anilino) naphthalene-5, 5′-disulfonic acid with α-crystallin. *J. Biol. Chem.* 273:8965–8970. https://doi.org/10.1074/jbc.273.15.8965.

38. Lee, J. S., J. H. Liao, …, S. H. Chiou. 1997. alpha-Crystallin acting as a molecular chaperonin against photodamage by UV irradiation. *J. Protein Chem.* 16:283–289. https://doi.org/10.1023/a:1026305025816.

39. Borkman, R. F., G. Knight, and B. Obi. 1996. The molecular chaperone α-crystallin inhibits UV-induced protein aggregation. *Exp. Eye Res.* 62:141–148. https://doi.org/10.1006/exer.1996.0018.

40. Lee, J. S., T. Satoh, …, S. H. Chiou. 1997. Effect of heat-induced structural perturbation of secondary and tertiary structures on the chaperone activity of α-crystallin. *Biochem. Bioph. Res. Co.* 237:277–282. https://doi.org/10.1006/bbrc.1997.7131.

41. Raman, B., and C. M. Rao. 1994. Chaperone-like activity and quaternary structure of α-crystallin. *J. Biol. Chem.* 269:27264–27268. https://doi.org/10.1016/s0021-9258(18)46978-5.

42. Das, K. P., and W. K. Surewicz. 1995. Temperature-induced exposure of hydrophobic surfaces and its effect on the chaperone activity of α-crystallin. *FEBS Lett.* 369:321–325. https://doi.org/10.1016/0014-5793(95)00775-5.

43. Reddy, G. B., P. Kumar, …, M. S. Kumar. 2006. Chaperone-like activity and hydrophobicity of alpha-crystallin. *IUBMB Life.* 58:632–641. https://doi.org/10.1080/15216540601010096.

44. Vanhoudt, J., S. Abgar, …, J. Clauwaert. 2000. Native quaternary structure of bovine alpha-crystallin. *Biochemistry.* 39:4483–4492. https://doi.org/10.1021/bi990386u.

45. Barth, A. 2007. Infrared spectroscopy of proteins. *Biochim. Biophys. Acta Bioenerg.* 1767:1073–1101. https://doi.org/10.1016/j.bbabio.2007.06.004.

46. Okuno, T. 1991. Thermal effect of infrared radiation on the eye-a study based on a model. *Ann. Occup. Hyg.* 35:1–12. https://doi.org/10.1093/annhyg/35.1.1.

47. Wang, B., C. Yu, …, L. X. Xie. 2010. A novel CRYGD Mutation (p.Trp43Arg) causing autosomal dominant congenital cataract in a Chinese family. *Hum. Mutat.* 32:1939–1947. https://doi.org/10.1002/humu.21386.

48. Li, S. S., Y. Y. Yu, …, Y. X. Weng. 2013. Thermal-induced unfolding of β-crystallin and disassembly of its oligomers revealed by temperature-jump time-resolved infrared spectroscopy. *Chinese J. Chem. Phys.* 26:739–746. https://doi.org/10.1063/1674-0068/26/06/739-746.

49. Li, S. S., R. Wang, …, Y. X. Weng. 2014. Thermal-triggerd proteinquake leads to disassembly of DegP hexamer as an imperative activation step. *Sci. Rep.* 4:4834. https://doi.org/10.1038/srep04834.

50. Li, H., Y. Wang, …, Y. Weng. 2020. Dynamical and allosteric regulation of photoprotection in light harvesting complex II. *Sci. China Chem.* 63:1121–1133. https://doi.org/10.1007/s11426-020-9771-2.

51. Yue, S., Z. Wang, …, Y. X. Weng. 2017. Coupling of multi-vibrational modes in bacteriochlorophyll *a* in solution observed with 2D electronic spectroscopy. *Chem. Phys. Lett.* 683:591–597. https://doi.org/10.1016/j.cplett.2017.03.029.

52. Li, D. Y., Y. Li, …, Y. X. Weng. 2015. A Q-switched Ho: YAG laser assisted nanosecond time-resolved T-jump transient mid-IR absorbance spectroscopy with high sensitivity. *Rev. Sci. Instrum.* 86:053105. https://doi.org/10.1063/1.4921473.

53. Han, J., and K. L. Schey. 2006. MALDI tissue imaging of ocular lens alpha-crystallin. *Invest. Ophthalmol. Vis.* 47:2990. https://doi.org/10.1167/iovs.05-1529.

54. Raman, B., T. Ramakrishna, and C. Mohan Rao. 1995. Temperature dependent chaperone-like activity of alpha-crystallin. *FEBS Lett.* 365:133–136. https://doi.org/10.1016/0014-5793(95)00440-k.

55. Kaiser, C. J. O., C. Peters, …, S. Weinkauf. 2019. The structure and oxidation of the eye lens chaperone αA-crystallin. *Nat. Struct. Mol. Biol.* 26:1141–1150. https://doi.org/10.1038/s41594-019-0332-9.

56. Jehle, S., P. Rajagopal, …, H. Oschkinat. 2010. Solid-state NMR and SAXS studies provide a structural basis for the activation of αB-crystallin oligomers. *Nat. Struct. Mol. Biol.* 17:1037–1042. https://doi.org/10.1038/nsmb.1891.

57. Braun, N., M. Zacharias, …, S. Weinkauf. 2011. Multiple molecular architectures of the eye lens chaperone αB-crystallin elucidated by a triple hybrid approach. *Proc. Natl. Acad. Sci. U.S.A.* 108:20491–20496. https://doi.org/10.1073/pnas.1111014108.

58. Barth, A., and C. Zscherp. 2002. What vibrations tell about proteins. *Q. Rev. Biophys.* 35:369–430. https://doi.org/10.1017/s0033583502003815.

59. Kubelka, J., and T. A. Keiderling. 2001. Differentiation of β-sheet-forming structures: ab initio-based simulations of IR absorption and vibrational CD for model peptide and protein β-sheets. *J. Am. Chem. Soc.* 123:12048–12058. https://doi.org/10.1021/ja0116627.

60. Arrondo, J. L. R., A. Muga, …, F. M. Goñi. 1993. Quantitative studies of the structure of proteins in solution by Fourier-transform infrared spectroscopy. *Prog. Biophys. Mol. Biol.* 59:23–56. https://doi.org/10.1016/0079-6107(93)90006-6.

61. Ye, M. P., H. Li, …, X. G. Qiu. 2007. Intermolecular hydrogen bonds formed between amino acid molecules in aqueous solution investigated by temperature-jump nanosecond time-resolved transient mid-IR spectroscopy. *Chinese J. Chem. Phys.* 20:461–467. https://doi.org/10.1088/1674-0068/20/04/461-467.

62. Yan, T., S. Li, …, B. Zou. 2012. Pressure-induced phase transition in N-H···O hydrogen-bonded molecular crystal oxamide. *J. Phys. Chem. B.* 116:9796–9802. https://doi.org/10.1021/jp302575k.

63. Tamm, L. K., and S. A. Tatulian. 1997. Infrared spectroscopy of proteins and peptides in lipid bilayers. *Q. Rev. Biophys.* 30:365–429. https://doi.org/10.1017/s0033583597003375.

64. Ghosh, A. 2019. Vibrational coupling on stepwise hydrogen bond formation of amide I. *J. Phys. Chem. B.* 123:7771–7776. https://doi.org/10.1021/acs.jpcb.9b05118.

65. Gruszecki, W. I., E. Janik, …, Z. Gryczynski. 2009. Supramolecular organization of the main photosynthetic antenna complex LHCII: a monomolecular layer study. *Langmuir.* 25:9384–9391. https://doi.org/10.1021/la900630a.

66. Lin, S. Y., M. J. Li, and C. J. Ho. 1999. PH-dependent secondary conformation of bovine lens alpha-crystallin: ATR infrared spectroscopic study with second-derivative analysis. *Graef. Arch. Clin. Exp.* 237:157–160. https://doi.org/10.1007/s004170050211.

67. Lima, E. C., A. A. Gomes, and H. N. Tran. 2020. Comparison of the nonlinear and linear forms of the van't Hoff equation for calculation of adsorption thermodynamic parameters (ΔS° and ΔH°). *J. Mol. Liq.* 311:113315. https://doi.org/10.1016/j.molliq.2020.113315.

68. Garvín, A., R. Ibarz, and A. Ibarz. 2017. Kinetic and thermodynamic compensation. A current and practical review for foods. *Food Res Int.* 96:132–153. https://doi.org/10.1016/j.foodres.2017.03.004.

69. Zhang, L., J. Yang, …, Y. X. Weng. 2003. Direct observation of interfacial charge recombination to the excited-triplet state in all-trans-retinoic acid sensitized TiO_2 nanoparticles by femtosecond time-resolved difference absorption spectroscopy. *J. Phys. Chem. B.* 107:13688–13697. https://doi.org/10.1021/jp035236e.

70. Walsh, M. T., A. C. Sen, and B. Chakrabarti. 1991. Micellar subunit assembly in a three-layer model of oligomeric α-crystallin. *J. Biol. Chem.* 266:20079–20084. https://doi.org/10.1016/s0021-9258(18)54893-6.

71. Augusteyn, R. C., and A. Stevens. 1998. Macromolecular structure of the eye lens. *Prog. Polym. Sci.* 23:375–413. https://doi.org/10.1016/s0079-6700(98)80008-7.

72. Morris, A. M., and J. A. Aquilina. 2010. Evidence for specific subunit distribution and interactions in the quaternary structure of α-crystallin. *Proteins.* 78:2546–2553. https://doi.org/10.1002/prot.22766.

73. Palmieri, V., G. Maulucci, …, M. De Spirito. 2013. α-Crystallin modulates its chaperone activity by varying the exposed surface. *Chem. bio. chem.* 14:2362–2370. https://doi.org/10.1002/cbic.201300447.

74. Haslbeck, M., S. Walke, …, J. Buchner. 1999. Hsp26: a temperature-regulated chaperone. *EMBO J.* 18:6744–6751. https://doi.org/10.1093/emboj/18.23.6744.

75. Eaton, W. A., V. Muñoz, …, J. Hofrichter. 2000. Fast kinetics and mechanisms in protein folding. *Annu. Rev. Biophys. Biomol. Struct.* 29:327–359. https://doi.org/10.1146/annurev.biophys.29.1.327.

76. Haslbeck, M., S. Weinkauf, and J. Buchner. 2019. Small heat shock proteins: simplicity meets complexity. *J. Biol. Chem.* 294:2121–2132. https://doi.org/10.1074/jbc.rev118.002809.

77. Shroff, N. P., S. Bera, …, E. C. Abraham. 2001. Substituted hydrophobic and hydrophilic residues at methionine-68 influence the chaperone-like function of alphaB-crystallin. *Mol. Cell. Biochem.* 220:127–133. https://doi.org/10.1023/a:1010834107809.

78. Posner, M., A. J. Kiss, …, Y. V. Sergeev. 2012. Functional validation of hydrophobic adaptation to physiological temperature in the small heat shock protein αA-crystallin. *PLoS One.* 7:e34438. https://doi.org/10.1371/journal.pone.0034438.

79. Biswas, A., S. Karmakar, …, K. P. Das. 2015. Interaction of α-crystallin with some small molecules and its effect on its structure function. *Biochim. Biophys. Acta Gen. Subj.* 1860:211–221.

80. Kosinski-Collins, M. S., S. L. Flaugh, and J. King. 2004. Probing folding and fluorescence quenching in human γD crystallin Greek

key domains using triple tryptophan mutant proteins. *Protein Sci.* 13:2223–2235. https://doi.org/10.1110/ps.04627004.

81. Davis, A. M., and S. J. Teague. 1999. Hydrogen Bonding, hydrophobic interactions, and failure of the rigid receptor hypothesis. *Angew. Chem. Int. Ed.* 38:736–749. https://doi.org/10.1002/(sici)1521-3773(19990315)38:6<736::aid-anie736>3.0.co;2-r.

82. Doss, E. W., K. A. Ward, and J. F. Koretz. 1997. Preliminary studies on the aggregation process of alpha-crystallin. *Exp. Eye Res.* 65:255–266. https://doi.org/10.1006/exer.1997.0337.

83. Lórenz-Fonfría, V. A., Y. Furutani, and H. Kandori. 2008. Active internal waters in the bacteriorhodopsin photocycle. A comparative study of the L and M intermediates at room and cryogenic temperatures by infrared spectroscopy. *Bio. chem.* 47:4071–4081. https://doi.org/10.1021/bi7024063.

84. Thöing, C., S. Oldemeyer, and T. Kottke. 2015. Microsecond deprotonation of aspartic acid and response of the α/β subdomain precede C-terminal signaling in the blue light sensor plant cryptochrome. *J. Am. Chem. Soc.* 137:5990–5999. https://doi.org/10.1021/jacs.5b01404.